RESPONSE OF TWO-WAY REINFORCED MASONRY INFILL WALLS UNDER BLAST LOADING

RESPONSE OF TWO-WAY REINFORCED MASONRY INFILL WALLS
UNDER BLAST LOADING

By:
NICHOLAS LEE SMITH
B.Eng. & Mgmt. (McMaster University)

A Thesis Submitted to the School of Graduate Studies in Partial Fulfilment of the
Requirements for the Degree of Master of Applied Science

McMaster University

MASTER OF APPLIED SCIENCE (2014) McMaster University

(CIVIL ENGINEERING) Hamilton, Ontario

Title: Response of Two-Way Reinforced Masonry Infill Walls under Blast Loading

Author: Nicholas Smith, B.Eng. & Mgmt. (McMaster University)

Advisors: Dr. M.J. Tait
Dr. W.W. El-Dakhakhni

Number of Pages: ix, 63

ABSTRACT

The increased public safety concerns to the consequences of deliberate and accidental explosions have led to the development of the Canadian (CSA S850-12) and American (ASCE 59-11) blast standards. There is an urgent need to investigate and quantify the response of structural components under such extreme loading conditions. This is especially important for masonry components, where research has been limited due to the misconception that masonry (both reinforced and unreinforced) is an inadequate material for blast hardening applications. The standards allow the use of experimental testing or dynamic analysis in order to determine peak responses and evaluate them in terms of the code prescribed performance limits and accompanying levels of damage. The current study investigates the response of non-integral and non-participating infill walls designed to undergo two-way out-of-plane response and detailed to fail in flexure under static loading conditions. Through experimental blast testing and dynamic model validation of reduced-scale walls under a range of design-basis threat (DBT) levels, this study shows that reinforced masonry is a viable alternative for blast protection. However, the current flexural-based code requirements, thought to be conservative, may be inadequate at loads of higher impulse where shear damage is prevalent. This study also shows the influence that changing the boundary configuration and level of reinforcement has on the peak response, where the performance limits of the current codes makes no provisions for these parameters.

ACKNOWLEDGEMENTS

This research was facilitated with funding provided by the Natural Sciences and Engineering Research Council of Canada (NSERC), McMaster University Centre for Effective Design of Structures (CEDS), funded through the Ontario Research and Development Challenge Fund (ORDCF), the Canadian Concrete Masonry Producers Association (CCMPA), and the Canada Masonry Design Centre (CMDC). The provision of mason time by Ontario Masonry Contractors Association (OMCA) is gratefully acknowledged. I am also grateful to the members of the Canadian Explosives Research Laboratory (CERL) who conducted the field blast tests and to the Canadian Forces for providing the range where the tests were conducted.

I would like to thank Dr. Tait and Dr. El-Dakhakhni for acting as my advisors and providing me with the much needed input, mentoring and sometimes motivation that was required to complete my thesis. The experimental work could not have been completed without the help of the other members of the McMaster Blast Team which included Brent Wybenga, Mostafa El-Sayed, Kevin Simonds and Mark Hayman as well as Ahmed Ashour and Omar El-Azizy who would take time away from their own work to help. Finally, I must extend a very special thank you to Kent Wheeler and Paul Hereema. Without their hard work and dedication none of this would have been a possibility.

I would like to thank Mr. David Stubbs and Dr. Bennett Banting of the Canada Masonry Design Centre for providing their supervision and technical expertise during the term of my Industrial NSERC Scholarship as well as the Ontario Masonry Training Centre for taking care of all my specimen construction and transportation logistics.

Finally, I would like to thank my family for always trying to push me to do bigger and better things, with a very special shout-out to Madeleine Joyal for putting up with all of my frustrations.

TABLE OF CONTENTS

LIST OF FIGURES

LIST OF TABLES

DECLARATION OF ACADEMIC ACHIEVEMENT

The experimental research and analysis presented in this thesis was carried out solely by Nicholas Smith (author) with mentorship and guidance from Dr. Michael Tait and Dr. Wael El-Dakhakhni who acted as academic supervisors while providing guidance and mentorship. Any outside sources of information used have been cited where applicable and all other materials are the sole work of the author.

CHAPTER 1: INTRODUCTION

1.1 Research Motivation

Access to once restricted information has facilitated the creation of explosive devices that can have detrimental implications on both a structure and its occupants. In the past, structural-blast performance has focused on military and post-disaster applications, with several technical manuals developed to outline methods of blast hardening for those facilities. However, increased occurrence of explosions and media coverage has created a public safety concern regarding the protection of civilian structures against blast, leading to the newly developed Canadian (CSA S850-12) and American (ASCE 59-11) blast standards. These performance-based design codes allow for all stakeholders of the structure to define the level of protection (LOP) they would like designed for with regards to an expected design-basis threat (DBT) level. Using these inputs, designers can consult the code resource materials, both qualitative and quantitative, to meet the target performance criteria.

The aforementioned blast standards currently allow for the performance of individual components (i.e. beam, column, wall, etc.) to be evaluated by either experimental blast testing or dynamic modelling. Using material specific performance limits, the standards relate the peak component response to prescribed levels of damage. The blast performance of most common construction materials (i.e. steel, concrete) is known to a relatively large degree, however, research in masonry is comparatively lacking due to misconception that masonry (both unreinforced and reinforced) is an inadequate material for blast hardening applications. This substantial lack of experimental data is a significant disadvantage when considering how extensively masonry construction is used in North America. Nonetheless, the standards do in fact prescribe performance limits and accompanying levels of damage for masonry assemblages even though the research that formed the basis for these requirements is limited.

It is the motivation of this study to build on the limited amount of research that currently forms the basis for the current blast code requirements. Through experimental testing and dynamic modelling, the author aims to show that reinforced masonry can be used as a viable blast hardening alternative as well as to provide additional data and analysis that can be used for future code modifications.

1.2 Theme and Layout of Thesis

This thesis has been assembled as a combination of two journal articles, with Chapters 2 and 3 presenting each of the papers in their entirety. The information in these chapters was primarily investigated and written by the author of this thesis (Nicholas Smith), who also acted as the principal author on both journal articles. The articles were co-authored by the thesis supervisors: Dr. M.J. Tait and Dr. W.W. El-Dakhakhni, as well as Dr. W.F. Mekky, all of whom acted as technical and editorial advisors. The objective of this research was to develop an increased understanding of the complex response invoked by blast loads through experimental testing and dynamic modelling of two-way reinforced masonry (RM) infill walls. Due to the limited research which provides for the basis of current code requirements, this study aims to provide recommendations for future code developments and enhancements in terms of blast-masonry interaction. To ensure the chapters can be read and understood independent of one-another, each chapter contains separate background information acting as a literature review. The reader will notice that certain themes in the background information have been repeated due to their significance in blast research as well as to both chapters, presented as stand-alone journal papers.

Chapter 2 presents the experimental results and analysis of blast testing nine RM infill walls from the journal article:

Smith, N. L., El-Dakhakhni, W. W., Tait, M. J., and Mekky, W. F. (2014). "Blast Performance Assessment of Two-Way Reinforced Concrete Block Infill Walls under Different Design-Basis Threat Levels." Submitted to *ASCE Journal of Structural Engineering* March, 2014.

The walls were reinforced in a doubly-symmetric manner, with support conditions detailed to invoke a two-way, out-of-plane flexural response. The objective of this paper was to develop an understanding of the blast response of two-way RM infill walls, as research into this area is significantly lacking. The study investigated the presence of shear damage in components that are designed and detailed to fail in flexure, which is known to arise in impulsive loads. This paper also aimed at comparing the qualitative and quantitative levels of damage observed from this testing, with the prescribed performance limits outlined in the current blast standards (ASCE 59-11 and CSA S850-12) and making recommendations for their future improvements.

Chapter 3 presents the development and results of a Single Degree of Freedom (SDOF) model which aimed to accurately simulate the out-of-plane dynamic response of two-way RM infill walls and is from the journal article:

Smith, N. L., Tait, M. J., El-Dakhakhni, W. W., and Mekky, W. F. (2014). "Response of Reinforced Concrete Masonry Infill Panels under Blast." Submitted to *ASCE Journal of Performance of Constructed Facilities* April, 2014.

The study aimed to simulate the peak response captured from the field blast testing through wall resistance functions that were measured experimentally and determined theoretically. Upon validating the model response with the results obtained through the field blast testing, the implications of the boundary conditions were investigated by modelling the same walls with differing support conditions. This aimed to bound the response of the ill-defined connections of non-integral and non-participating RM infill walls between two well-defined and commonly studied boundary conditions. This paper also investigated the development of full-scale performance charts (P-I diagrams) for a range of design-basis threat (DBT) levels. Through comparison of the iso-damage curves at unique levels of reinforcement, the paper suggested improvements to both the performance limits and charts currently used in code applications.

CHAPTER 2: EXPERIMENTAL PERFORMANCE

This chapter presents the experimental results and pertaining analysis of two-way reinforced masonry infill walls that were subjected to blast loads through free-field explosive testing. The information in this chapter is the sole information of the author, with Dr. W.W. El-Dakhakhni and Dr. M.J. Tait acting as both advisors and editors in the preparation of the journal manuscript. This chapter consists of the same information and structure that was presented in the journal submission:

Smith, N. L., El-Dakhakhni, W. W., Tait, M. J., and Mekky, W. F. (2014). "Blast Performance Assessment of Two-Way Reinforced Concrete Block Infill Walls under Different Design-Basis Threat Levels." Submitted to *ASCE Journal of Structural Engineering* March, 2014.

PAPER ABSTRACT: With the introduction of the two new North American standards for blast resistant design of buildings (ASCE 59-11 and CSA S850-12), there is a need to investigate and quantify the response of different structural components under such extreme loading conditions. Past studies on the response of masonry under blast have focused on the strengthening and retrofit aspects of existing unreinforced masonry (URM) components, whereas research studies related to quantifying the blast resistance of reinforced masonry (RM) have been significantly limited due to the perception that concrete block construction in general (both RM and URM) is hazardous under blast loads. As such, the focus of this study is on evaluating the performance of scaled RM walls under blast and comparing the observed performance to the limits prescribed in the ASCE 59-11 and CSA S850-12. The tests included a range of charge weights and wall capacities, representing different design-basis threat (DBT) levels (scaled-distances as low as a 1.61 m/kg$^{1/3}$) and expected levels of protection (LOP), respectively. The test results showed that a combined flexural-shear response governed the wall failure modes. At the lowest DBT level, support rotations approached 1.5°, which remained below the prescribed 2° threshold for Heavy damage, as was also confirmed through visual observation of the tested walls. At the highest DBT level considered, support rotations exceeded 7°. However, due to the wide range of support rotation limits between the code performance levels, the damage would still be classified as Heavy (as opposed to Hazardous) although the walls appeared to experience a significant loss of structural integrity. This study forms a part of an on-going research program that is aimed at facilitating better

understanding of RM component performance under a range of DBT levels. The reported results are also expected to contribute to the growing RM blast performance database in order to facilitate further development of RM design clauses in future editions of the ASCE 59-11 and CSA S850-12.

2.1 Introduction

Blast loads have the potential of inflicting high levels of damage to property and occupants if the safety of the structural system is compromised. As structural designers are typically concerned with hardening of key structural components to safely resist design-basis threats (DBT), it is necessary to recognize the importance of maintaining the building functionality and minimizing injuries and casualties due to non-structural component failures. In blast design, the term hardening is used to refer to any means taken in order to mitigate the effects of blast loading. This includes strengthening and stiffening of components as well as the use of barricades to limit the distance between the explosives and the targets. As structural frame buildings are widely used in traditional construction, non-loadbearing masonry infill walls are used extensively throughout North America and are typically constructed from concrete blocks. Although unreinforced masonry (URM) infill walls are more dominant, in seismic zones, such infill walls would typically be reinforced in both directions to minimize seismic hazard associated with URM. With infill walls comprising a large portion of the building envelope area, they form the first line of defense, which make them highly vulnerable to explosions and result in large displacement demands invoked in their out-of-plane direction. In addition, recent studies have shown that infill walls can be as critical for the structural integrity of the building as it is for the safety of its occupants. For example, infill walls have been recently shown to increase structural system robustness and reduce the probability of progressive collapse (Farazman et al. 2013; Mosalam and Gunay 2014).

Past research in the area of blast load-structure interaction has mainly focused on military applications and post-disaster facilities, where the considered assets were deemed to have a high DBT level (e.g. embassies) or a high level of importance (e.g. defense, emergency, government, and critical services). This has led to the development of several documents describing analysis techniques and providing guidelines pertaining to how these particular types of structures could be hardened against explosions (U.S. Department of the Army 1986; 1999; 2006; 2008). More recently, in response to an increased demand for higher general public safety levels, there has been a greater focus on advancing the knowledge pertaining to behaviour and performance of typical civilian structures to blast loads. The most recent major developments in North America include the release of specialized design codes, including both the American ASCE 59-11 (ASCE 2011) and the Canadian CSA S850-12 (CSA 2012) blast standards. These performance-based standards call for the input of the facility owners, users, and other stakeholders to specify the level of protection (LOP) that they require their facility to be designed for and also provide significant resource materials, both qualitative and quantitative, in order to enable designers to fulfill the necessary target performance criteria.

As blast response evaluation and enhancement of non-military structural components are relatively new areas of research when compared to the current knowledge base pertaining to their response under other forms of dynamic loading (e.g. wind and seismic), both the breadth and depth of experimental data is relatively lacking. Compared to other components, research on masonry response to blast has been limited due to not only to the complexity of testing but also because of the general perception that masonry, both reinforced and unreinforced, is not a suitable construction material for blast resistant applications. The tests reported by Dennis et al. 2002, Baylot et al. 2005, and Abou-Zeid et al. 2011 have utilized simple boundary conditions to invoke one-way behaviour and subject masonry walls to an array of charge weights and standoff distances to cover a range of DBT levels and induce different damage levels. The test results facilitated an advanced understanding of the response of concrete block masonry wall systems to such extreme loading events and demonstrated that, with proper design, masonry construction has the potential to be a viable blast resistant system.

In the test program described herein, the response of two-way reinforced concrete block masonry infill walls was investigated through experimental testing of nine reduced-scale wall specimens with three different reinforcement ratios. The walls were subjected to varying charge sizes located at the same standoff distance in order to investigate a range of DBT levels that would induce different displacement demands on the infill walls (Wu and Hao 2007). The findings presented in this paper are based on detailed observations and analyses of the walls' displacement response data and the walls' post-blast damage levels following each blast shot. In order to augment these findings, the following section gives a brief description of the main characteristics of blast loads as a background.

2.2 Blast Load Characteristics

Upon detonation of an explosive device, a sudden release of energy generates a high velocity–supersonic shock wave front that travels by continuously compressing the air in front of it (Baker 1973). This shock wave front typically travels in a spherical trajectory where, after a certain propagation distance, the pressure wave becomes almost planar leading to the simplified assumption of a uniform pressure distribution on the surface of the target under consideration (Baker et. al 1983). The corresponding wave front parameters are typically referred to as the far-field blast load characteristics. Free-air explosions are those where the charge centre is at a significant distance from any reflective surface (including the ground), resulting in a spherical blast wave moving away from the charge centre in all directions (Baker et al. 1983). Alternatively, surface blasts result from the charge centre being in direct contact or in close proximity to a surface (e.g. the ground), resulting in a hemispherical blast wave. For both the spherical and hemi-spherical explosions, the reflected blast pressure becomes significantly larger than the incident overpressure due to an energy funnelling caused by the reflection (Baker et al. 1983). For simplification, an ideal air blast has been typically modelled using the Modified Friedlander Equation given by:

$$P(t) = P^{+}\left(1 - {}^{t}/_{t_d}\right) \mathrm{e}^{\left(-{}^{\alpha t}/_{t_d}\right)} \tag{2.1}$$

where $P(t)$ is the blast pressure at any time t; and is a function of the peak overpressure P^{+}; the positive phase duration t_d; and a curve fitting parameter α (Baker et al. 1983). The Modified Friedlander Equation indicates an instantaneous increase in the blast overpressure, which is commonly referred to as a zero rise-time, followed by an exponential decay through the positive phase and into a negative (suction) phase before returning to the ambient pressure as depicted in Fig. 2.1. As the peak negative pressure and associated specific impulse (the area of the pressure response history within the negative phase) are often significantly lower than their corresponding positive counterparts, the former are commonly ignored in the component response analysis. This simplification is also conservative as the peak component response typically occurs in the first cycle, where accounting for the negative impulse would reduce the component response.

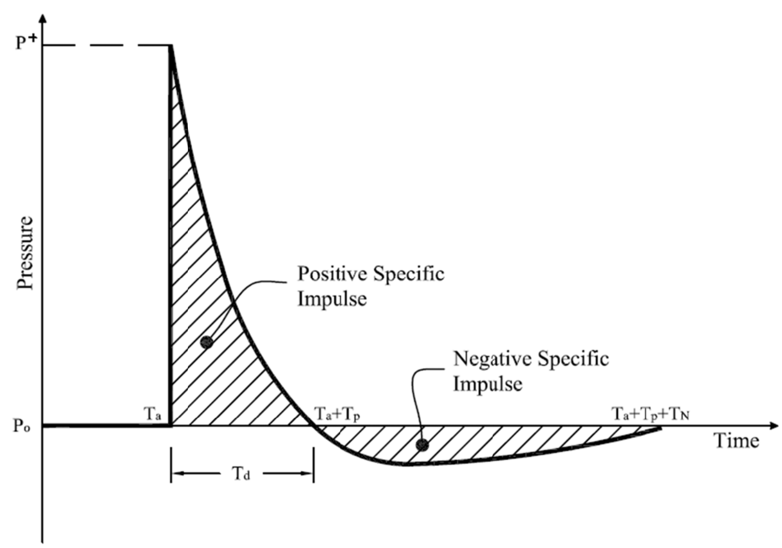

Figure 2.1. Ideal Pressure-Time History

A key parameter in the study of component response to explosive loads is referred to as the scaled-distance. One of the most common scaling techniques used in blast load quantification and normalization is known as the cube-root scaling rule developed by Hopkinson (1915) and is given by:

$$Z = R/W^{1/3} \tag{2.2}$$

where *Z* is the scaled-distance parameter; *R* is the standoff distance between the charge centre and the specimen; and *W* is the explosive charge weight.

The scaled-distance approach is a convenient way to both quantify the explosion effects (as it accounts for both the charge weight and the standoff distance) as well as to compare different DBTs, with smaller *Z* values being more detrimental. As such, several combinations of unique standoff distances and explosive charge weights (and thus DBT levels) can result in identical scaled-distance values. Subsequently for the same *Z* value, self-similar blast wave characteristics would develop, the most important of which is the peak side-on overpressures (Baker et al. 1983). Researchers studying blast-structure interaction utilize this phenomenon by replicating the overpressure resulting from very large explosive charges with smaller charge sizes by simply reducing the distance between the charge centre and the target. This has significant implications on both the test costs and the safety associated with explosive testing. As a commonly accepted normalization approach, all charge weights are expressed in terms of their TNT equivalent in order to compare the effect of different explosive types. A TNT equivalency ratio is based on the relative total energy released as well as the heat of combustion of the reaction (Baker et al. 1983) in order to more easily draw comparison between the observed responses and those expected to result from the extensively studied TNT explosive. However, for the blast wave characteristics to be similar under the same scaled-distance, the explosion has to fall within the far-field explosion category, within which, the uniformity of the blast wave front parameter can be assumed. This can be considered achieved when the scaled-distance, Z, is larger than 1.2 m/kg$^{1/3}$ (Dusenberry 2010).

2.3 Experimental Program

The scaled walls tested in this study were chosen to model a 3.0 m long and 3.0 m high prototype reinforced masonry (RM) infill wall constructed using standard 190 mm concrete blocks. These blocks are commonly used in a running bond configuration within steel and concrete frame construction throughout North America. In order to conform to the test site limitations on charge size, third-scale wall specimens were constructed using one-third scale true-replicas of the standard 190 mm concrete block units. Scaled models present a useful tool in evaluating the response of structural components to blast loads, however it is critical that the scaling effects be considered when developing the test program, and interpreting and analyzing the test results. Table 2.1 shows the relationship between the full- and the reduced-scale model parameters (Harris and Sabnis 1999), where the variable λ represents the ratio between the scaled-model dimension and the full-scale prototype dimensions, which is equal to 1/3 in the current study. Subsequently, the reduced-scale walls were 1.0 m long x 1.0 m high x 63 mm thick.

Table 2.1. Full- and Reduced-Scale Relationships

Parameter	Full-scale Value	Scale-model Value
Dimension	x	λx
Area	A	$\lambda^2 A$
Volume	V	$\lambda^3 V$
Time	t	λt
Scaled Distance	Z	Z
Pressure	P	P
Impulse	I	λI

Note: $\lambda = 1/3$ for current test program

2.3.1 Test Setup and Instrumentation

The ill-defined boundary conditions of a typical infill wall that is non-integral (i.e. with no physical connections with the surrounding frame) and non-participating (i.e. not in full contact with the top and side frame members as per seismic detailing requirement), presented an experimental simulation challenge. This is because, without well-defined boundary conditions, a major source of uncertainty will be introduced and significant difficulties would subsequently develop when interpreting the test results. As such, the focus was to prevent possible wall arching, under out-of-plane bending, which would further complicate interpreting the wall response and deviate from the non-participating infill wall construction. Subsequently, only the wall corners were supported causing the wall to deflect in a dome-like shape as shown in Fig. 2.2.

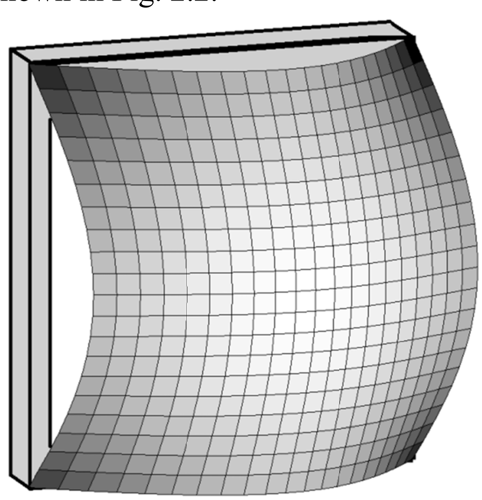

Figure 2.2. Idealized Deflected Shape

The steel test bunker, illustrated in Figs. 2.3-a and 2.3-b, was constructed to serve multiple purposes during the test program. Firstly, it provided a reaction frame for the walls under blast load by imposing the necessary boundary conditions where, in order to allow the specimen to undergo the required response (Fig. 2.2), steel caps (made of C-sections) were fitted to each wall corner and used to transfer the wall reactions to the blast bunker frame as depicted in Fig. 2.3-c. These steel corner caps were placed flush against a 50 mm solid steel round bar, which was positioned at a 45° angle and attached rigidly to the test bunker frame to simulate a rotationally unrestrained hinge support.

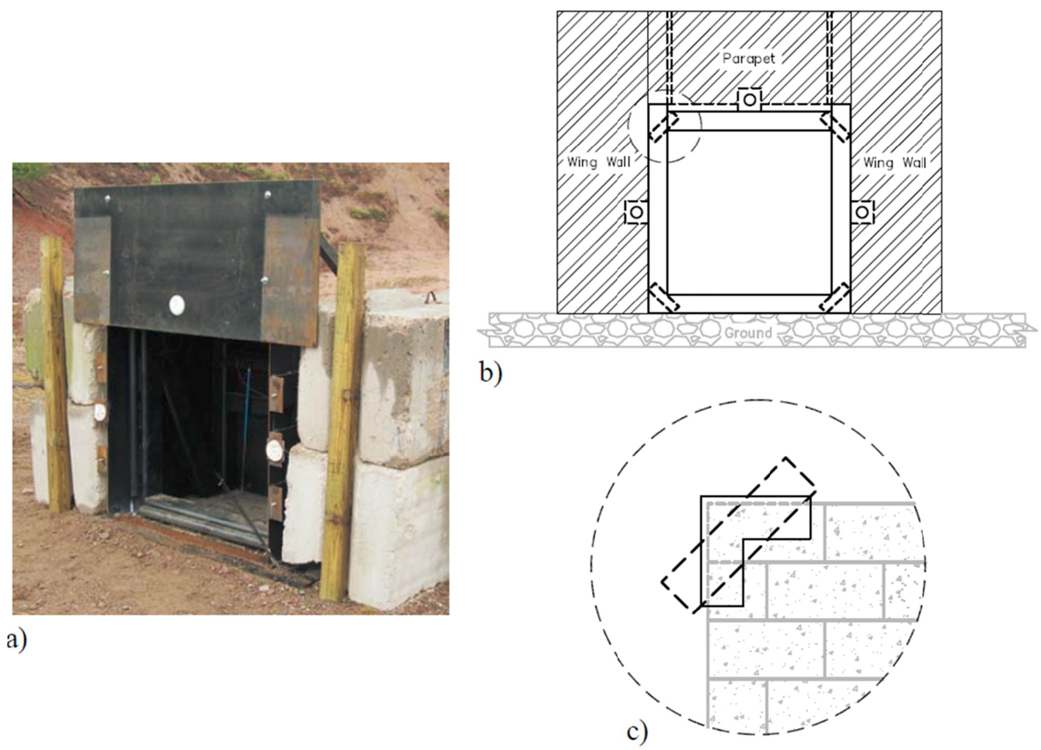

Figure 2.3. Test Bunker: a) On-Site Configuration; b) Illustration Facing Charge Centre; c) Wall Connection Detail

The steel test bunker also facilitated mitigating two commonly occurring blast phenomena, which can result in undesirable effects during blast tests, known as the wrap-around (engulfing) and the clearing effects. The wrap-around (engulfing) effect refers to the high incident pressure waves traveling behind the target, thus imposing pressure on its rear face, which decreases the target response and leads to fictitiously higher capacities (Ballantyne et al. 2010). As such, using the boxtype steel bunker mitigated this effect. Unlike the wrap-around effect that tends to decrease the net pressure on the target through the pressure wave traveling behind it, the clearing effect results in a decreased pressure on the front surface of the target due to the target's finite size. This is attributed to the fact that, near the free edges, rarefaction waves are produced and propagate towards the centre of the target, causing interference and decreasing the peak over-pressure to which the target is subjected (Ballantyne et al. 2010). In order to mitigate this effect, a steel top parapet and side wing walls (Fig. 2.3-b) were sized based on ConWep (Hyde 1990) calculations in order to ensure an almost uniform pressure and impulse over the entire wall (target) surface. Sample ConWep (Hyde 1990) analysis results, shown in Fig. 2.4, indicates that the selected sizes of the top parapet and wing walls resulted in a maximum difference in the pressure values over the wall surface of 8% at all charge sizes.

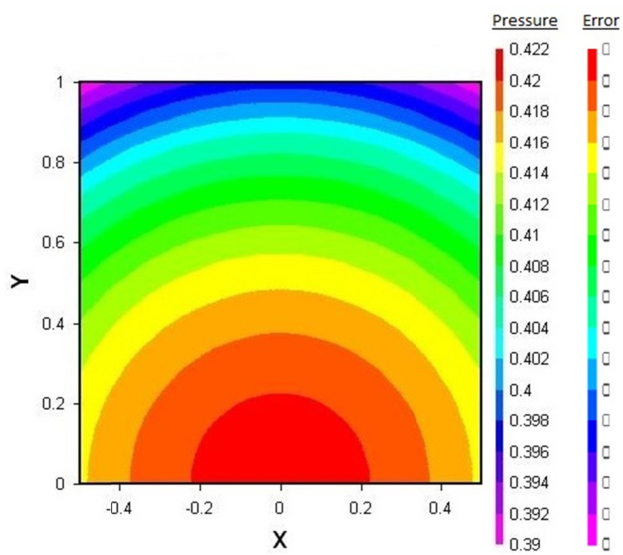

Figure 2.4. Predicted Pressure Distribution (Z=2.75 m/kg$^{1/3}$)

Linear variable differential transducers (LVDTs) were used to capture the deflection response of the wall specimens during each event as their relative rigidity and robustness made them ideal for accurately capturing the rapid response. These transducers had a stroke length of 300 mm and a data sampling rate of 1 MHz, allowing for a significant number of readings to capture the wall response history. Each transducer was attached to the rear of the wall specimen (i.e. the side facing opposite to the charge) as well as the rigid test bunker frame and were all positioned in a quarter-grid pattern as shown in Fig. 2.5-a to depict the walls' deflected shapes. The pressure transducers, attached to the bunker frame directly adjacent to the walls as depicted in Fig. 2.5-b, collected the reflected pressure data on the specimen at a data sampling rate of 1 MHz.

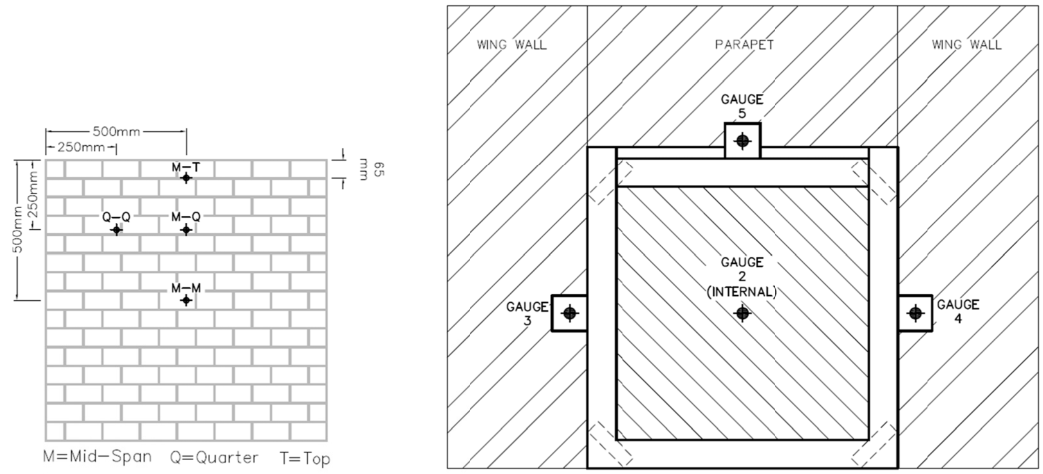

a) b)

Figure 2.5. Instrumentation Layout: a) LVDTs; b) Pressure Gauges

2.3.2 Material and Test Matrix

In order to test a range of wall designs and DBT scenarios, the nine scaled walls were constructed with three different reinforcement ratios, to be subjected to three different charge sizes (while maintaining a constant standoff distance). As such, by changing the reinforcement ratios, comparisons could be drawn between the relative capacities of each wall specimen tested under a specific charge weight. On the other hand, for walls with the same reinforcement ratio, damage levels can be monitored under increased charge weights. The three charge sizes, representing a range of DBT levels, were made of Pentex^{TM} Duo 16-454 Cast Booster, which has a TNT equivalency ratio of 1.2 (Orica 2010). As such, the 5, 10 and 25 kg charge sizes resulted in equivalent TNT weights of 6, 12 and 30 kg with each set of three walls (the three different reinforcement ratios) being subjected to the same explosive charge size.

All walls were fully-grouted and reinforced in a doubly symmetric manner (vertically and horizontally) with deformed reinforcing steel of either type D4 (area = 25 mm^2) or D7 (area = 45 mm^2). These bar sizes were chosen as they represent an intermediate and a practical upper range on reinforcement that can be utilized in hardened RM construction at full-scale. The material properties of the individual constituents were evaluated according to the respective CSA and ASTM standards (CSA 2004a; CSA 2004b; ASTM 2012). The walls were constructed with scaled concrete blocks having an average compressive strength of 20.1 MPa, and a coefficient of variation (COV) of 12% as well as mortar and grout with strengths of 28.1 MPa (COV=10%) and 23.2 MPa (COV=12%), respectively. These constituent materials resulted in an average fully-grouted masonry prism strength of 18.2 MPa (COV=11%) and a Young's modulus of 14,300 MPa (COV=14%). A consistent mortar and grout mix design was used throughout the construction stages, ensuring that the aggregate sizes were scaled accordingly (Harris and Sabnis 1999). The ratios, given in terms of mass of cement-lime-sand-water, were 1.0: 0.2: 3.53: 0.85 for mortar and 1.0: 0.04: 3.9: 0.85 for grout (CSA 2004b). The average yield strengths of the reinforcing bars were tested to be 478 MPa (COV=1%) and 484 MPa (COV=4%) for the D4 and D7 bars, respectively.

The test matrix is presented in Table 2 outlining each wall type as well as the equivalent TNT charge weight and corresponding scaled-distance.

Table 2.2. Test Matrix

Wall	**Reinforcement Ratio, ρ (%)**	**Equivalent TNT Charge Mass (kg)**	**Scaled Distance, Z (m/kg$^{1/3}$)**
WNL-6	0.32	6	2.75
WNM-6	0.59	6	2.75
WNH-6	1.07	6	2.75
WNL-12	0.32	12	2.18
WNM-12	0.59	12	2.18
WNH-12	1.07	12	2.18
WNL-30	0.32	30	1.61
WNM-30	0.59	30	1.61
WNH-30	1.07	30	1.61

It is worth noting that the scaled-distances for each blast scenario are above the 1.2 m/kg$^{1/3}$ threshold for far-field blast wave characteristics (Dusenberry 2010) as was discussed previously. This was expected to facilitate the assumption of a planar, self-similar blast pressure wave. The wall types are labeled starting by "WN" as these wall specimens were planned as a part of a larger test program that included other wall types. The character that follows is used to distinguish between the level of reinforcement (***L***ow, ***M***oderate or ***H***igh) and the appended number represents the explosive charge size in kg of TNT. As an example, WNL-6 represents the walls with a Low reinforcement ratio (D4 bar in every-other vertical cell and horizontal course) subjected to an equivalent TNT charge weight of 6 kg, while WNM-12 and WNH-30 represent the walls with a Moderate (D4 bar in every vertical cell and horizontal course) and High (D7 bar in every vertical cell and horizontal course) reinforcement ratio respectively and subjected to equivalent TNT charge weights of 12 and 30 kg, respectively. Fig. 2.6-a depicts a typical specimen with the steel corner caps whereas Fig. 2.6-b demonstrates schematic placements of the steel reinforcing bars in the walls, clearly showing the two-way symmetrical reinforcing pattern.

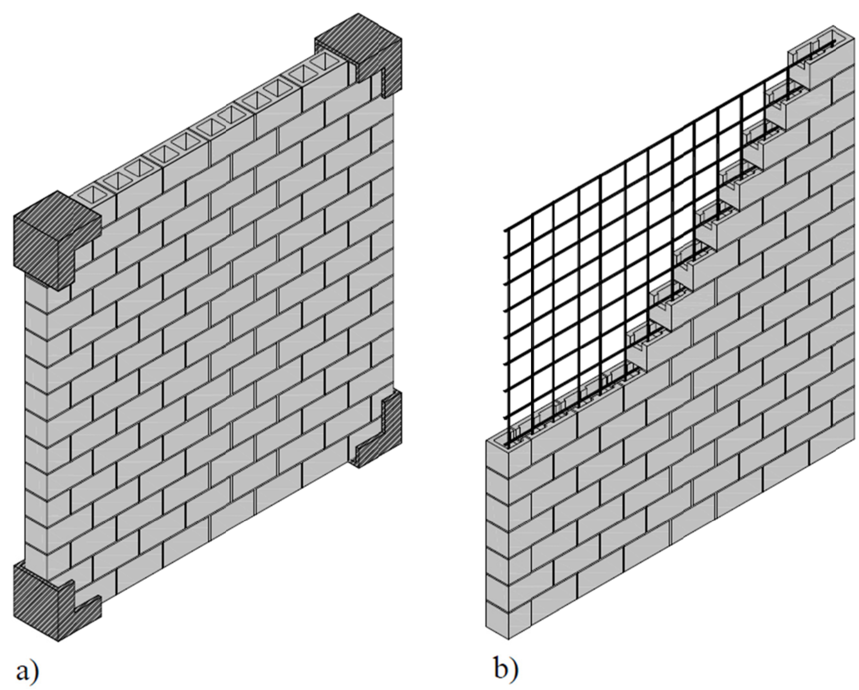

Figure 2.6. Infill Wall Specimen: a) Boundary Conditions; b) Steel Reinforcement Mesh

2.4 Experimental Results

2.4.1 Pressure Profiles

Three pressure transducers were used to record the pressure histories at various locations on the test bunker frame surrounding the test specimens, as depicted in Fig. 2.5-b, to capture the reflected pressure history. This pressure is significantly larger than the pressure at the wave front, which is referred to as the incident pressure (Baker et al. 1983). Due to ringing of the gauges as a result of the vibration following the arrival of the blast wave, it was difficult to accurately quantify experimental values for the peak pressure and to some extent, the positive phase durations by simply observing the pressure histories. As such, numerical integration of each experimental pressure history was performed to measure the cumulative impulse, with its maximum value representing the end of the positive phase duration as can be seen in Fig. 2.7. Subsequently, least-squares regression analyses using the Modified Friedlander Equation (Baker et al 1983) were performed, using the obtained positive phase durations, to determine the peak pressure, P^+, and the corresponding specific impulse, I^+ values. An example of the Modified Friedlander Equation fit is shown is Fig. 2.7 and the fit results are outlined in Table 2.3 along with the experimentally evaluated positive phase duration and impulse as applicable. During the WNM-30 wall test the transducers had malfunctioned, resulting in no pressure data being captured.

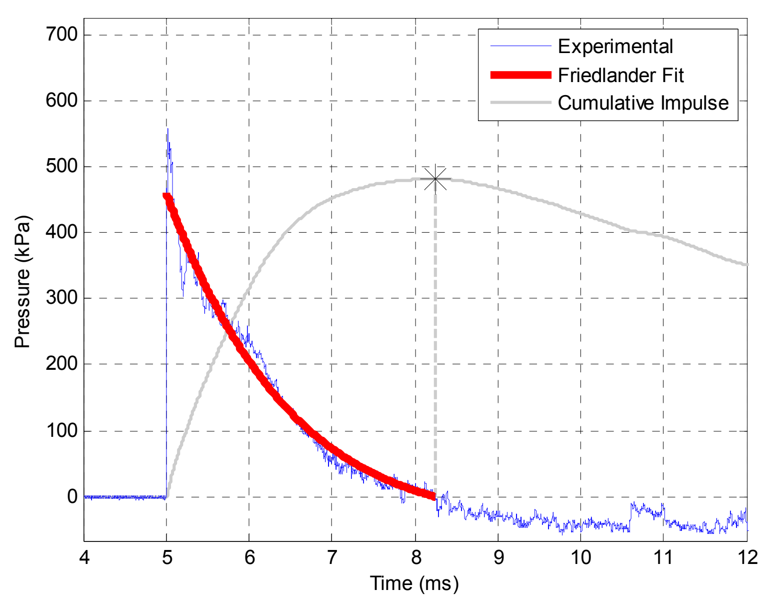

Figure 2.7. Sample Pressure-Time History (WNL-6)

Table 2.3. Pressure-Time History Parameters

Wall	***Experimental***		***Fit***	
	Impulse, I^+ (kPa.ms)	**Duration, t_d (ms)**	**Pressure, P^+ (kPa)**	**Impulse, I^+ (kPa.ms)**
WNL-6	482	3.23	460	489
WNM-6	463	3.15	405	466
WNH-6	396	2.97	343	402
WNL-12	617	3.22	698	628
WNM-12	709	2.28	871	702
WNH-12	595	1.87	780	581
WNL-30	1836	6.61	1927	1718
WNM-30*	-	-	-	-
WNH-30	2291	6.79	2304	2019

*Pressure Transducers data acquisition module malfunctioned

2.4.2 Post-blast Observations

The post blast damage patterns of the specimens are shown Fig. 2.8. Only the rear sides of the walls (i.e. the side facing opposite to the charge) are depicted, as this is where the majority of wall damage developed. Photograph inserts depicting the front of the wall are used to highlight significant features as applicable. By grouping the wall specimens based on the same scaled-distance values, it is observed that consistent trends in damage modes develop regardless of the reinforcement ratio, where most of the walls experienced combined shear and flexural damage. Fig. 2.8-a depicts the three tests that were performed at the smallest charge size (largest scaled-distance of 2.75 $m/kg^{1/3}$) and shows that damage was primarily observed as a result of shear near the support locations. It is hypothesized that the lack of flexural damage (cracks near the mid-spans) is the result of the blast load not being large enough to invoke the necessary displacement demand at the wall mid-span to cause significant cracking. Although damage did not appear to be attributed to flexural action, the wall deflection responses, as will be discussed later, show that the specimens did in fact undergo significant out-of-plane deformations.

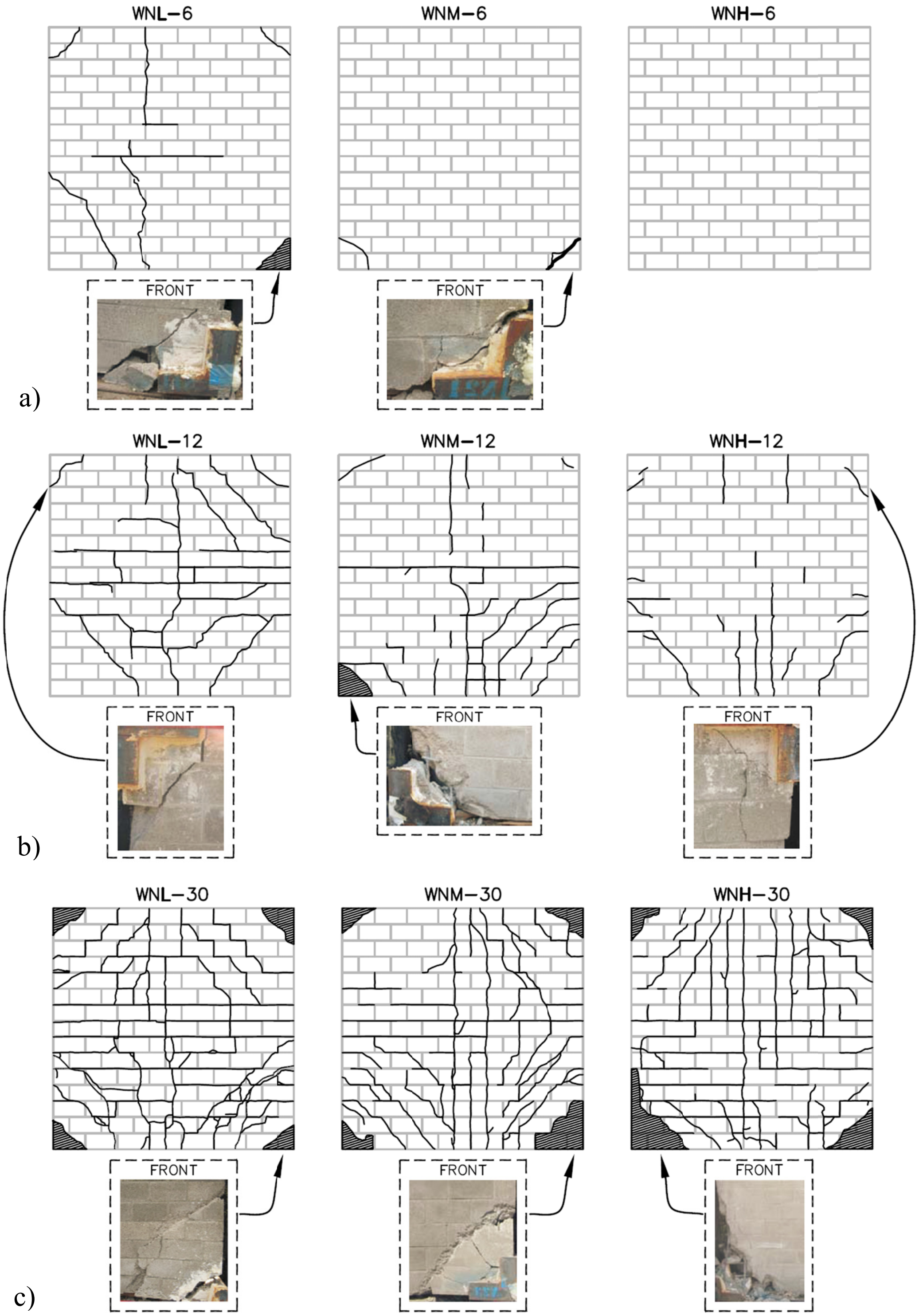

Figure 2.8. Damage Patterns:
a) Z=2.75 m/kg$^{1/3}$; b) Z=2.18 m/kg$^{1/3}$; c) Z=1.61 m/kg$^{1/3}$

Fig. 2.8-b illustrates the results of the three specimens that were tested at the intermediate charge size (scaled-distance of 2.18 m/kg$^{1/3}$). Under this scaled distance, evidence of combined shear-flexural damage patterns were observed. The flexural damage is exhibited in the horizontal and vertical cracks at the wall mid-spans as well as concentric circular-type cracks originating at both central region and wall support locations. This is seen more predominantly in Wall WNL-12 as it had the lowest reinforcement ratio. Diagonal cracks near the supports indicate damage development due to the shear mechanism. Despite the fact that at support locations there was some signs of damage, it was evident that the post-blast structural integrity was maintained and the wall did not experience rigid body motion throughout the duration of its response history. As was expected, the level of plastic deformation in the walls varied depending on the level of reinforcement, with the specimen having the lowest reinforcement ratio (WNL-12) experiencing the highest level of damage. This was also apparent following the analysis of the deflection response histories of the individual wall specimens, as discussed later in the paper.

Fig. 2.8-c shows the damage patterns for the three specimen tests that were tested under the largest charge size (scaled-distance of 1.61 m/kg$^{1/3}$). Depictions of severe damage on the front face of the walls are shown through the insert photographs. Similar to the wall results under the intermediate charge size, there is strong evidence of combined shear-flexural damage. As in the previous group of tests, flexure is shown through the prominent vertical and horizontal cracks at the wall central regions as well as the concentric circular cracks, although these are more severe due to the increased charge size. The plastic deformation resulting from the flexural action was so severe that the specimens had a permanent dome-like shape at the conclusion of the test. Similar to walls subjected to the intermediate charge size, diagonal cracking parallel to the support locations was observed in these walls as well. The significant difference with these specimens is the extent of their damage near the support locations. The lightly reinforced Wall WNL-30 experienced rupturing of the steel reinforcement at these locations resulting in a loss of post-blast structural integrity and a change in the deformed shape early on in its response. This level of damage was starting to develop with Walls WNM-30 and WNH-30, however, the increased reinforcement ratios in these two walls provided sufficient resistance to maintain their post-blast structural integrity. The post-blast permanent deformation of Wall WNH-30 (with the largest reinforcement ratio) confirmed the wall's improved performance compared to the others subjected to the same charge size. Due to the

loss of structural integrity of WNL-30 (with the lowest reinforced ratio), it is hypothesized that the wall experienced a rigid body motion throughout the rest of its response history from the significant relative displacement between the corner zones and the rest of the wall.

2.4.3 Displacement Response Histories

The quarter grid pattern of the LVDTs previously shown in Fig. 2.5-a was used to capture the deflection response of the specimens during and after the blast event. As a typical response history, the results of the WNL-12 specimen are shown in Fig. 2.9.

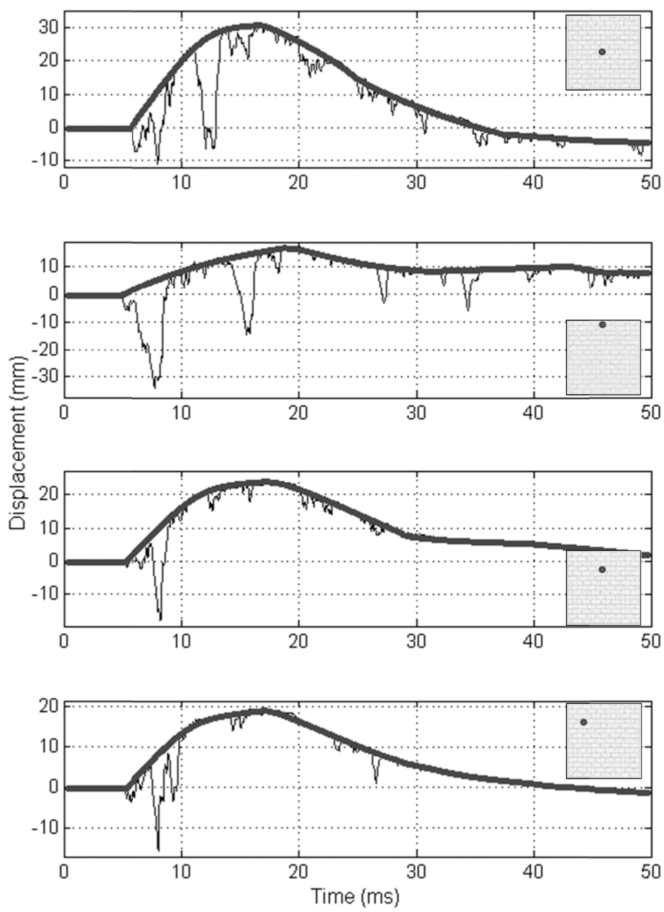

Figure 2.9. Sample Deflection Responses (WNL-12)

Due to the intense percussion and accompanied vibration generated by the detonation of the explosive, some minimal distortion is observed over the deflection response history. To facilitate visualization, the assumed symmetric deflection profiles through the wall vertical centreline as well as diagonally across the each wall's supports are shown in Fig. 2.10, where the expected effects of the reduced reinforcement ratio (and thus lesser wall capacity) and the reduced scaled-distance (corresponding to a higher DBT), are apparent from the subsequent increase in the walls' mid-span deflections. Table 2.4 summarizes the peak deflections recorded at the wall specimen centres.

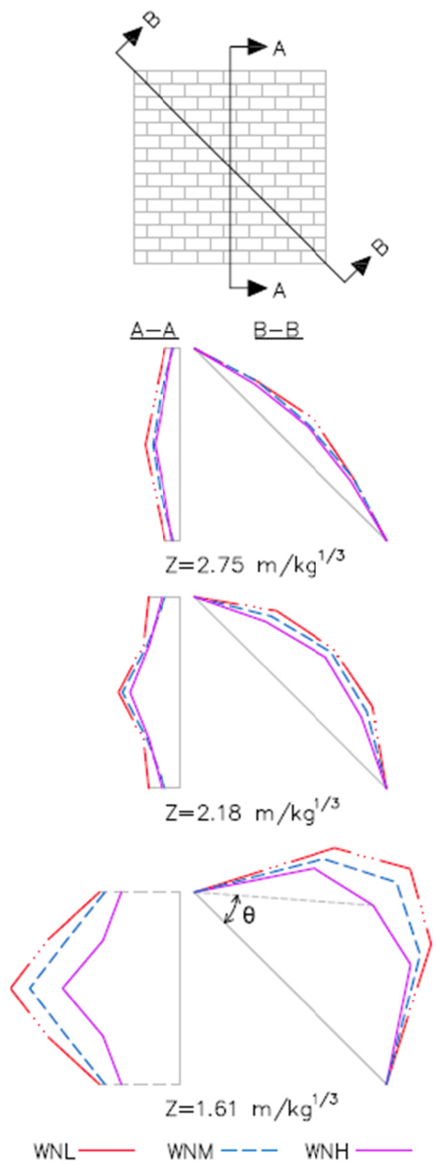

Figure 2.10. Deflection Profiles (Relative Scale)

Table 2.4. Peak Experimental Wall Responses

Wall	Mid-Point Deflection (mm)	Chord Rotation, θ	Prescribed Damage Level
WNL-6	18	1.5°	Moderate
WNM-6	14	1.1°	Superficial
WNH-6	13	1.0°	Superficial
WNL-12	32	2.6°	Heavy
WNM-12	30	2.5°	Heavy
WNH-12	26	2.1°	Heavy
WNL-30	88	7.1°	Heavy
WNM-30*	78	6.3°	Heavy
WNH-30	67	5.4°	Heavy

*Extrapolated from other LVDT measurements

2.5 Analysis of Experimental Results

Evaluation of the deflection and pressure histories reveals that, as expected, the time taken by each wall to reach its maximum displacement is longer than the entire positive phase duration of the blast event. This confirmed the assumptions that the walls would respond in their impulsive loading regime (Baker et. al 1983) under the different scaled-distances reported in the current study. As a result, the corresponding wall response would be dependent on the specific impulse (area under the pressure history) rather than the peak pressure value.

2.5.1 Influence of Test Parameters on the Expected Wall Response

The damage modes of fully-grouted RM construction share similar characteristics with those observed in their reinforced concrete (RC) counterparts. In this regard, it has been shown through experimental testing (Fujikura and Bruneau 2011) and numerical modelling (Shi et al. 2008) that the mode of failure of RC components can significantly change depending on the scaled-distance. One example of this is the recently reported study on the blast response of seismically detailed, ductile RC bridge piers and columns that were designed and detailed to fail in flexure (Fujikura and Bruneau 2011). In that study, it was observed that the RC specimens experienced significant levels of shear damage near the supports when loaded within their impulsive loading regime. This type of damage is attributed to the fact that impulsive loads, with a large amplitude and short duration, can force shear stresses to rapidly reach high levels well before large flexural deformations develop (Shi et al. 2008). Static testing using an air bag conducted by Smith et al. (2014) on RM walls similar to those reported in the current study have shown that, when subjected to uniform static pressure under the same boundary conditions, these infill walls would indeed fail in flexure with no shear damage occurring near the supports as can be seen in Fig. 2.11. Due to the extreme dynamic nature of the impulsive blast loads and the corresponding dynamic reaction at the wall support, coupled with the relatively high stiffness of fully-grouted RM components, it was expected that both shear and flexural damage patterns might develop within the blast tested walls simultaneously.

a) b)

Figure 2.11. Static Test Damage Patterns: a) Rear of Wall; b) Side Profile

The deflection profile of the wall specimens resulted in prominent vertical and horizontal cracks along the wall centrelines as well as concentric circular/rhombic cracks within the walls' central regions and near the supports as depicted in Fig. 2.12-a. Although there was a significant level of flexural cracking throughout the wall, shear cracks appeared to be concentrated at critical planes (see Fig. 2.12-b) near the supports, where the demand exceeded the wall's shear capacity. With the further development of flexural action, a combined shear-flexural damage pattern materializes as depicted in Fig. 2.12-c which is also consistent with observations of blast loaded square RC panels (Razaqpur et al. 2009).

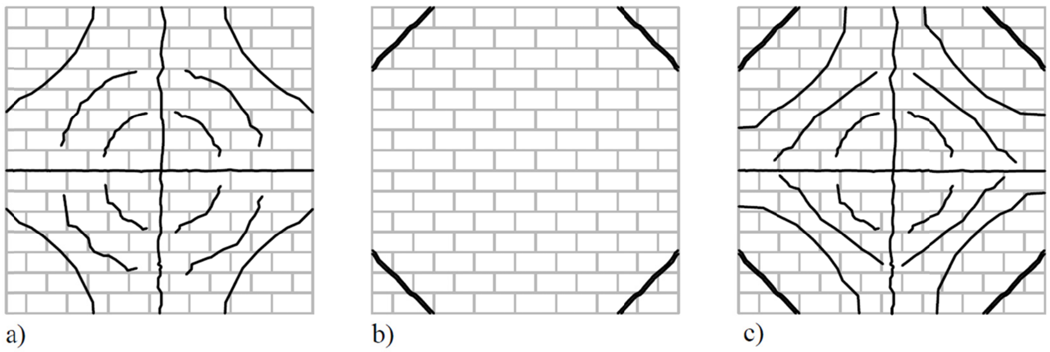

Figure 2.12. Idealized Rear Damage Patterns: a) Flexure; b) Shear; c) Combined Flexure-Shear

To visualize the different parameter effects on the response of the walls, Fig. 2.13 depicts the effects of the steel ratios and scaled-distances on the peak chord rotation. For clarity, the wall response surface in Fig. 2.13-a is presented for specific reinforcement ratios in Fig. 2.13-b and specific scaled-distances in Fig. 2.13-c. The wall chord rotation response values shown in Fig. 2.13-b appear to be a function of the scaled-distance regardless of the reinforcement ratio. In general, at the lower range of scaled-distances the chord rotation is more sensitive to the variation in the scaled distance, as is evident by the steeper slope which reflects the significant effects of reducing scaled-distance under higher DBT levels compared to lower ones.

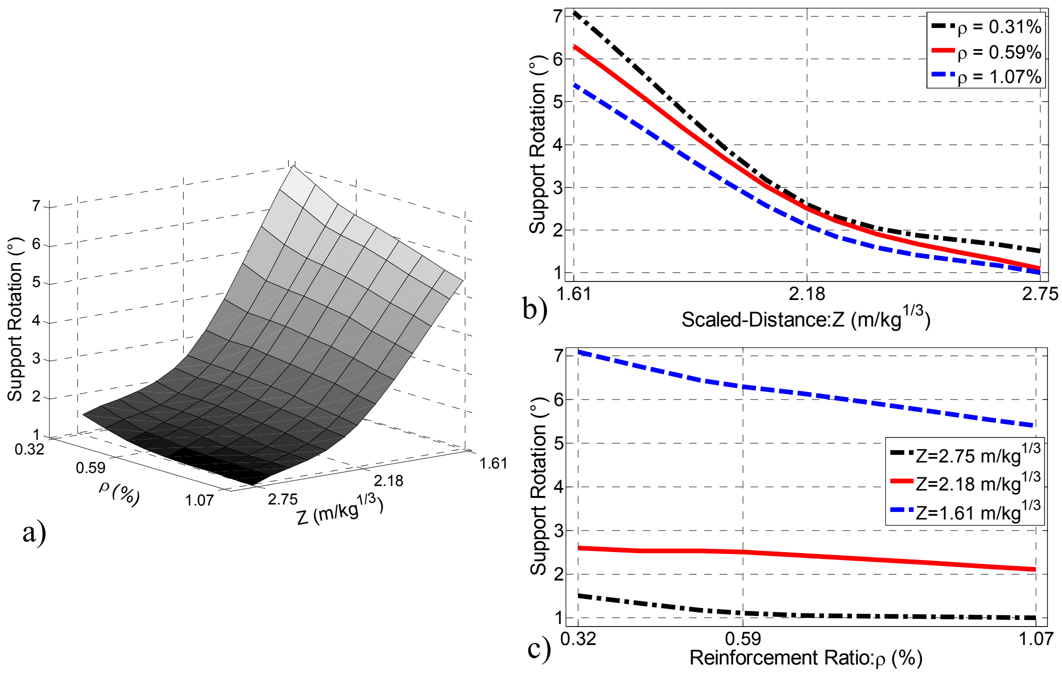

Figure 2.13. Effect of Test Parameters on Support Rotation: a) Combined; b) Reinforcement Ratio; c) Scaled-Distance

2.5.2 ASCE and CSA Performance Limits

The American ASCE 59-11 (ASCE 2011) and Canadian CSA S850-12 (CSA 2012) blast standards define threshold damage levels and corresponding performance limits when analyzing the response of reinforced masonry walls. These parameters *implicitly* assume flexural response, as shear is typically a brittle and undesirable failure mechanism. This however, might prove to be unrealistic as even when designed and detailed to develop a flexural failure, there is always a possibility for shear failure to develop under blast loading (Shi et al. 2008; Fujikura and Bruneau 2011). Based on the currently reported test results, an attempt to relate the ASCE 58-11 and CSA S850-12 performance limits/damage levels (listed in Table 2.5) to the wall deflection response reported earlier in Table 2.4. These damage levels range from *Superficial,* which indicates minor cosmetic damage, to a *Blowout*, which indicates a complete loss of structural integrity. The majority of the quantitative limits are defined by the maximum chord rotation θ_{max} at the support except in the case of the *Moderate* damage threshold, which is identified by yielding of the reinforcement and a subsequent permanent deformation (μ=1).

Table 2.5. Code Prescribed Damage Levels

Code Damage Level	Response Limit, θ_{max}
Superficial	-
Moderate (B1)	-
Heavy (B2)	2°
Hazardous (B3)	8°
Blowout (B4)	15°

To facilitate comparison, the peak deflections from the wall displacement response histories were converted to an approximate support rotation by taking the arctangent of the ratio of the deflection to the effective deflected length. This effective length was selected to be the diagonal distance from the centre of the wall support to the wall central point as this is considered to be perpendicular to the major axis of rotation and would thus be more reflective of the wall's support conditions. This approach is considered to be a suitable estimate of damage when plastic deformation is prominent in both the ASCE 59-11 (ASCE 2011) and the CSA S850-12 (CSA 2012) blast standards.

By using the code performance (rotation) limits outlined previously, each wall was assigned a damage level as prescribed by the blast standards (ASCE 2001; CSA 2012). As can be inferred from Table 2.4, the walls with higher steel reinforcement ratios tended to have lower rotations and in turn a more desirable LOP under all DBT levels studied, as was expected. At the largest scaled-distance (i.e. lowest DBT) the specimens underwent minimal rotations, which allowed for the damage to be classified as *Superficial* on the WNM-6 and WNH-6 walls. The exception occurs with the lightly reinforced WNL-6 specimen being classified *Moderate* as permanent deformations were observed from the wall displacement response history.

It is worth noting that, under the lowest scaled-distance (i.e. highest DBT), the range of chord rotations, as calculated, is quite high as a result of the shear deformation (essentially a rigid body deformation) having a significant contribution to the overall wall central point displacement. Under such circumstances (i.e. when shear significantly influence the wall chord rotation value), the wall reinforcement ratio (although mainly selected to meet specific flexural capacity requirements) plays a major role in minimizing shear failureinduced deformations by providing resistance through shear-friction and dowel action (CSA 2004c) as the masonry shear capacity deteriorates at the shear failure plane. This may explain why the lightly reinforced walls (WNL-30 and WNM-30) underwent significantly larger central point displacements than the WNH-30 as a result of the wall damage depicted previously in Fig. 2.8. As such, using the code classification of damage (ASCE 2011; CSA 2012), all walls tested under the intermediate and lowest scaled-distances (i.e. intermediate and largest DBT) would be classified under *Heavy* damage regardless of their reinforcement ratio. However, by observing the damage patterns previously depicted in Fig. 2.8, it can be inferred that the smallest scaled-distance (i.e. largest DBT) resulted in a damage level that visually appears to be quite hazardous, essentially approaching the *Blowout* code level. As such, unless the numerical chord rotation threshold values are both related to more quantitative indicators and explicitly restricted to pure flexural and excludes other failure modes (e.g. combined shear-flexural), these prescribed code threshold values may result in an unconservative damage assessment.

2.6 Conclusions

The blast response of two-way RM infill walls is evaluated through testing of nine reduced-scale walls with different reinforcement ratios and design-basis threat (DBT) levels. The blasts were generated through live explosive charges resulting in scaled-distances ranging between 2.75 m/kg$^{1/3}$ and 1.61 m/kg$^{1/3}$, with peak reflected pressures and specific impulses ranging from approximately 340 kPa to 2,300 kPa and from 400 kPa.ms to 2,300 kPa.ms, respectively.

At the lowest DBT level (Z=2.75 m/kg$^{1/3}$) the wall chord rotations ranged between 1.0° and 1.5°, which the current blast standards (ASCE 2011 and CSA 2012) prescribe as *Superficial* to *Moderate* damage and was verified through visual observation of tested specimens. The walls tested under the intermediate DBT level (Z=2.18 m/kg$^{1/3}$) exhibited chord rotations ranging from 2.1° to 2.6°, classifying their response under the *Heavy* damage level as per the standards. Finally, the highest DBT level (Z=1.61 m/kg$^{1/3}$) resulted in wall support rotations between 5.4° and 7.1°. As was the case with the moderate DBT level, these numerical threshold-based performance limits fall within the *Heavy* damage classification even though visual inspection showed that these walls possessed very little, if any, post-blast structural integrity. The reason for this perceived under-classification of damage levels results from the performance limits being implicitly based on flexural response without accounting for combined failure modes (e.g. shear-flexure) even though previously reported blast studies have shown their significance. This study has shown that when subjected to impulsive loads, similar to their RC counterparts, RM wall response and ultimate damage might be governed and significantly affected by a combined shear-flexure response. This indicates the need to revisit current code quantitative performance threshold provisions and inclusion of more qualitative performance assessment criteria. Along with other reported studies, the current test results demonstrate the need to account for blast-specific failure modes (i.e. influence of shear) that arise due to different levels of impulse and may neither be predicted through static testing nor mitigated through subsequent detailing.

2.7 Notation for Chapter 2

E	=	elastic modulus;
f'_m	=	average compressive strength of four course masonry prisms;
f_u	=	ultimate stress of reinforcing bars;
f_y	=	yield stress of reinforcing bars;
I^+	=	positive specific impulse of blast;
$P(t)$	=	blast pressure;
P^+	=	peak overpressure of blast;
R	=	standoff distance;
t_d	=	positive phase duration;
W	=	charge weight;
Z	=	scaled-distance;
α	=	exponential shape factor;

2.8 References for Chapter 2

Abou-Zeid, B. M., El-Dakhakhni, W. W., Razaqpur, A. G., and Foo, S. (2011). "Response of arching unreinforced concrete masonry walls to blast loading." *J. Struct. Eng.*, 137(10), 1205-1214.

American Society of Civil Engineers (ASCE). (2011). "Blast protection of buildings." *ASCE 59-11*, Reston, VA.

ASTM (2012). "Standard specification of deformed and plain carbon-steel bars for concrete reinforcement." *A615-12*, Conshohocken, PA.

Baker, W. E. (1973). "Explosions in Air." University of Texas Press. Austin, TX.

Baker, W. E., Cox, P. A., Westine, P. S., Kulesz, J. J., and Strehlow, R. A. (1983). "Explosion hazard and evaluation", Elsevier, Amsterdam.

Ballantyne, G., Whittaker, A., Dargush, G., Aref, A. (2010). "Air-blast effects on structural shapes of finite width." *J. Struct. Eng.*, 136(2), 152-159.

Baylot, J. T., Bullock, B., Siawson, T. R., and Woodson, S. C. (2005). "Blast response of lightly attached concrete masonry unit walls." *J. Struct. Eng.*, 131(8), 1186–1193.

Canadian Standards Association (CSA). (2004a). "Masonry construction for buildings." *CSA A371-04*, Mississauga, ON, Canada.

Canadian Standards Association (CSA). (2004b). "Mortar and grout for unit masonry." *CSA A179-04*, Mississauga, ON, Canada.

Canadian Standards Association (CSA). (2004c). "Design of masonry structures." *CSA S304.1-04*, Mississauga, ON, Canada.

Canadian Standards Association (CSA). (2012). "Design and assessment of buildings subjected to blast loads." *CSA S850-12*, Mississauga, ON, Canada.

Dennis, S. T., Baylot, J. T., and Woodson, S. C. (2002). "Response of ¼-scale concrete masonry unit (CMU) walls to blast." *J. Eng. Mech.*, 128(2), 134-142.

Dusenberry, D.O. (2010). "Handbook for Blast Resistant Design of Buildings." New-Jersey, USA: Wiley & Sons Inc., First Edition.

Farazman, S., Izzuddin, B., and Cormie, D. (2013). "Influence of unreinforced masonry infill panels on the robustness of multistory buildings." *J. Perform. Constr. Facil.*, 27(6), 673–682.

Fujikura, S. and Bruneau, M. (2011). "Experimental investigation of seismically resistant bridge piers under blast loading." *J. Bridge Eng.*, 16(1), 63-71.

Harris, H. G., and Sabnis, G. M. (1999). "Structural Modelling and Experimental Techniques", 2nd Ed., CRC Press, Boca Raton, FL.

Hopkinson, B. (1915). *British Ordinance Board Minutes 13565*.

Hyde, D. (1990). "User's guide for microcomputers programs CONWEP and FUNPRO-applications of TM 5-855-1." Experimental Station, U.S. Army Engineers Waterways, Vicksburg, MS.

Mosalam, K. M. and Gunay, S. (2014). "Progressive collapse analysis of RC frames with URM infill walls considering in-plane/out-of-plane interaction." *Earthquake Spectra In-Press*.

Newmark, N. M. (1972). "External blast." *State-of-the-Art Rep. No. 7, ASCE-IABSE Int. Conf. on the Planning and Design of Tall Buildings*, ASCE, New York, Vol. 1b, 661–676.

Orica. (2010) "Pentex™ duo 16-454 cast booster: technical data sheet" located at www.oricaminingservices.com.

Razaqpur, A. G., Contestabile, E., and Tolba, A. (2009). "Experimental study of the strength and deformations of carbon fiber reinforced polymer (CFRP) retrofitted reinforced concrete slabs under blast load." *Canadian Journal of Civil Engineering*, 36(8), 1366-1377.

Shi, Y., Hao, H., and Li, Z-X. (2008). "Numerical derivation of pressure-impulse diagrams for prediction of RC column damage to blast loads." *J. Impact Eng.*, 35(11) 1213-1227.

Smith, N. L., Tait, M. J., El-Dakhakhni, W. W., and Mekky, W. F. (2014). "Response of Reinforced Concrete Masonry Infill Panels under Blast." Submitted to *ASCE Journal of Performance of Constructed Facilities* April, 2014.

U.S. Department of the Army. (1986). "Fundamentals of protective design for conventional weapons." *TM 5-855, U.S. Department of the Army Technical Manual*, Washington, D.C.

U.S. Department of the Army. (1999). "Structures to resist the effects of accidental explosions." *TM 5-1300, U.S. Department of the Army Technical Manual*, Washington, D.C.

U.S. Department of the Army. (2006). "Minimum Anti-Terrorism Standards for Buildings." *UFC 4-010-01, U.S. Department of the Army Technical Manual*, Washington, D.C.

U.S. Department of the Army. (2008). "Design of structures to resist the effects of accidental explosions." *UFC 3-340-02, U.S. Department of the Army Technical Manual*, Washington, D.C.

Wu, C. and Hao, H. (2007). "Safe scaled distance for masonry infilled RC frame structures subjected to airblast loads." *J. Perform. Constr. Facil.*, 21(6), 422–431.

CHAPTER 3: DYNAMIC ANALYSIS

This chapter presents the development, results and pertaining analysis of blast loaded, two-way reinforced masonry infill walls through Single Degree of Freedom (SDOF) dynamic modelling. The information in this chapter is the sole information of the author, with Dr. M.J. Tait and Dr. W.W. El-Dakhakhni acting as both advisors and editors in the preparation of the journal manuscript. This chapter consists of the information and structure presented in the journal submission:

Smith, N. L., Tait, M. J., El-Dakhakhni, W. W., and Mekky, W. F. (2014). "Response of Reinforced Concrete Masonry Infill Panels under Blast." Submitted to *ASCE Journal of Performance of Constructed Facilities* April, 2014.

PAPER ABSTRACT: Increased exposure to the detrimental effects of blast events has led to the release of several guidelines (U.S. Department of the Army 1986; 1999; 2006; 2008) and the publication of recent standards (ASCE 2011; CSA 2012) that provide guidance on the hardening and performance quantification of structures subjected to this type of loading. The safety, security logistics, and the high cost associated with performing experimental blast testing has led to a number of codes and guidelines accepting the use of simplified dynamic modeling techniques in order to analyze the response of structural components. Past research in blast-masonry interaction has primarily focused on the strengthening and retrofit of existing unreinforced masonry (URM) wall systems, whereas research related to evaluating the blast response of reinforced masonry (RM) has been limited. The focus of this study is to evaluate the accuracy of using simplified dynamic modelling techniques to predict the blast performance of non-integral, RM infill walls. To evaluate the accuracy of the simplified dynamic models, the predicted response values are compared with results obtained from experimental blast testing of RM that cover a range of wall design parameters, charge weights and a constant standoff distance. The combinations of charge weights and standoff distance presented a range of scaled-distances, reflecting different explosive threat levels which were selected to induce different damage levels in the RM walls. Results from this study indicate that the wall peak deflection response can be accurately predicted using simplified dynamic models. Additionally, it was found that the complex response of the non-integral infill walls investigated in this study is bounded by two common boundary

configurations as verified by further analyses and Pressure-Impulse (P-I) diagrams. The analysis results are expected to provide a better understanding of RM infill wall performance under blast loads and the performance charts can be used as a screening tool for existing walls and preliminary design of new construction under different design-basis threat levels.

3.1 Introduction

Traditionally, research into blast-structure interaction was reserved primarily for military and post-disaster applications with a focus on structures deemed to have an increased level of threat (e.g. governmental) or a high level of importance (e.g. emergency and critical services). This led to the development of several technical manuals outlining design and analysis techniques as well as guidelines as to how these structures could be blast hardened (U.S. Department of the Army 1986; 1999; 2006; 2008). More recently, in response to increased public safety concerns pertaining to deliberate and accidental blast events, significant advances have been made regarding blast protection for civilian structures with the release of specialized design codes including the recently adopted American (ASCE 2011) and Canadian (CSA 2012) blast standards. In order to meet structural component and overall system performance requirements, these standards allow for the use of dynamic modelling to capture component peak response; this is typically completed through Single (SDOF) or Multi (MDOF) Degree of Freedom analysis. Although the blast performance of common components is well documented, this analysis is a necessity for less common configurations and materials in which research is significantly lacking, as in the case of masonry components. The benefit of using a dynamic model becomes increasingly apparent when considering the significant safety and security requirements, and expense that are typically associated with experimental blast testing.

The design-basis threat (DBT) level of an explosive event is typically quantified through the scaled-distance parameter. Cube-root scaling (Hopkinson 1915) is one of the most common techniques and calculates the scaled-distance Z as the ratio of the standoff distance R to the cubic root of the explosive charge weight W as shown in Equation 3.1.

$$Z = R/_{W^{1/3}} \tag{3.1}$$

Several combinations of unique explosive weights and standoff distances can be found to yield an identical scaled-distance, representing a particular DBT level and resulting in the same peak blast pressure. This is advantageous as large explosive events can be replicated with smaller charge sizes by reducing the distance between the charge center and the structure. Within the recent standards (ASCE 2011 and CSA 2012), identification of a maximum DBT level is critical in determining the necessary design resistance in order to meet the specified performance limits.

Conventional beam-column frames are a commonly used structural system that allows for the efficient transfer of forces through relatively light and slender components. The slenderness of these framed members leads to the extensive use of non-loadbearing infill walls, typically constructed from concrete block masonry, to cover a significantly large area of the building envelope. Due to this configuration, infill walls can be highly vulnerable to exterior explosions and can experience significant response in their out-of-plane direction. Although these infill walls are widely used, research into blast-masonry interaction is limited due in part to the misconception that masonry walls (including reinforced masonry walls) present an inadequate construction system for blast applications as a result of the defined discontinuities that arise from the pre-formed blocks/mortar interfaces. Recently, a number of research studies (Dennis et al. 2002; Henderson et al. 2003; Baylot et al. 2005; and Abou-Zeid et al. 2011) have been undertaken in an attempt to better understand the out-of-plane performance of masonry walls when subjected to blast loads through testing of basic boundary conditions and wall configurations. Although focusing on the simplified one-way action of masonry walls, these studies provide a basis for understanding and predicting the response of these systems to blast loads and more importantly have shown that, with proper design, masonry has the potential to be a viable blast-resistant and hardening construction system.

3.2 Focus of Current Study

This study builds on experimental blast test results in which the complex out-of-plane blast response of non-integral (i.e. with no physical connections with the surrounding frame) and non-participating (i.e. not in full contact with the top and side frame members to meet seismic detailing requirement), reinforced masonry (RM) infill walls was investigated through scaled-specimens using simplified boundary conditions (Smith et al. 2014). By varying both the reinforcement ratio as well as the charge size, the wall specimens were subjected to a range of explosive threat levels invoking different responses and damage levels. Wall displacements were restricted at the corners only, where the free rotation about the supports resulted in a two-way flexural type response. Consistent with observations seen in the blast response of concrete columns (Shi et al. 2008) and bridge piers (Fujikura and Bruneau 2011), the specimens showed significant signs of shear damage at large impulse values even though they were designed and detailed to fail in flexure under static loading. The occurrence of this damage mode is attributed to the fact that impulsive loads, consisting of a large amplitude and short duration, result in sharp increases in shear stress prior to the development of flexural action (Shi et al. 2008).

With the prototype infill walls chosen to be 3.0 m in both length and height and constructed of a single 190 mm concrete block wythe, the one-third scale wall specimens used in the experimental blast testing were each 1.0 m in both length and height and were constructed using a single scaled block wythe of 63 mm in thickness. As the peak pressure remains constant at the same scaled-distance (Baker et. al 1973), the time and hence impulse (area under pressure-time history) of the replica wall can be scaled by the dimension factor, λ equal to 1/3, to reproduce similar results of the corresponding full-scale specimens (Harris and Sabnis 1999). Relevant parameters are presented in Table 3.1 (Harris and Sabnis 1999) showing the relationship between the full- and reduced-scale replica models.

Table 3.1. Full- and Reduced-Scale Relationships

Parameter	**Full-scale Value**	**Scale-model Value**
Dimension	x	λx
Area	A	$\lambda^2 A$
Volume	V	$\lambda^3 V$
Density	ρ	ρ
Mass	M	$\lambda^3 M$
Time	t	λt
Displacement	u	λu
Velocity	$\dot{u}$	$\dot{u}$
Acceleration	$\ddot{u}$	$\ddot{u}/\lambda$
Standoff	R	λR
Charge Weight	$W^{1/3}$	$\lambda W^{1/3}$
Scaled Distance	Z	Z
Pressure	P	P
Impulse	I	λI

Note: $\lambda = 1/3$ for current test program

The high stiffness of the RM walls leads to the response being primarily captured by the first mode, where a simplified Single Degree of Freedom (SDOF) model is considered to be acceptable for blast response modelling (Biggs 1964). As such, a dynamic model was developed in order to validate the experimental results as well as predict the wall response to DBT levels outside the range of the experimental program. Equations 3.2 and 3.3 show the equivalency of the reduced-scale (*r*) and full-scale (*f*) models through manipulation of the equations of motion using the relationships outlined in Table 3.1. In Eqs. 3.2 and 3.3, M, K, P and A are the mass, stiffness, blast load and surface area respectively with $\ddot{u}$ and u representing the system acceleration and displacement.

$$M_r\ddot{u}_r + K_r u_r = PA_r \tag{3.2}$$

$$\lambda^2 M_f \ddot{u}_f + \lambda^2 K_f u_f = \lambda^2 PA_f \tag{3.3}$$

Since the peak blast response typically occurs within the first cycle, before the effects of damping are initiated, the contribution of damping to the system response is typically neglected (Biggs 1964). As will be described in the following sections, validation of the experimental results is achieved through replicating the wall resistance functions, which were obtained through the static testing of identical walls as well as theoretical calculations. The developed SDOF models are then subjected to pressure-time histories that were both measured during the experimental testing as well predicted from the charge weight and standoff distance using the program ConWep (Hyde 1990).

3.3 Static Testing

3.3.1 Theoretical Capacity Predictions

In the field blast testing study (Smith et al. 2014), three different reinforcement ratios were used for the walls. To predict the theoretical out-of-plane static flexural capacities of the three wall types, a yield line approach, based on the virtual work method, was used in a similar manner to the analysis of two-way reinforced concrete slabs (Park and Gamble 2000). Estimates of the primary yield lines were determined through visual observation of the blast tested specimens (Smith et. al 2014). As Fig. 3.1-a illustrates, the theoretical yield lines consist of one vertical and one horizontal crack located at the mid-spans as well as diagonal cracks parallel to the wall rotational axes at the supports. As a result, the theoretical out-of-plane flexural capacity can be expressed in terms of an applied uniform pressure W_{fl} by:

$$W_{fl} = 16M_u/L^2 \tag{3.4}$$

where M_u is the one-way, out-of-plane ultimate moment resistance, which is equal in both directions as a result of the double symmetry of the wall reinforcement, and L is the length of the square specimen (1.0 m).

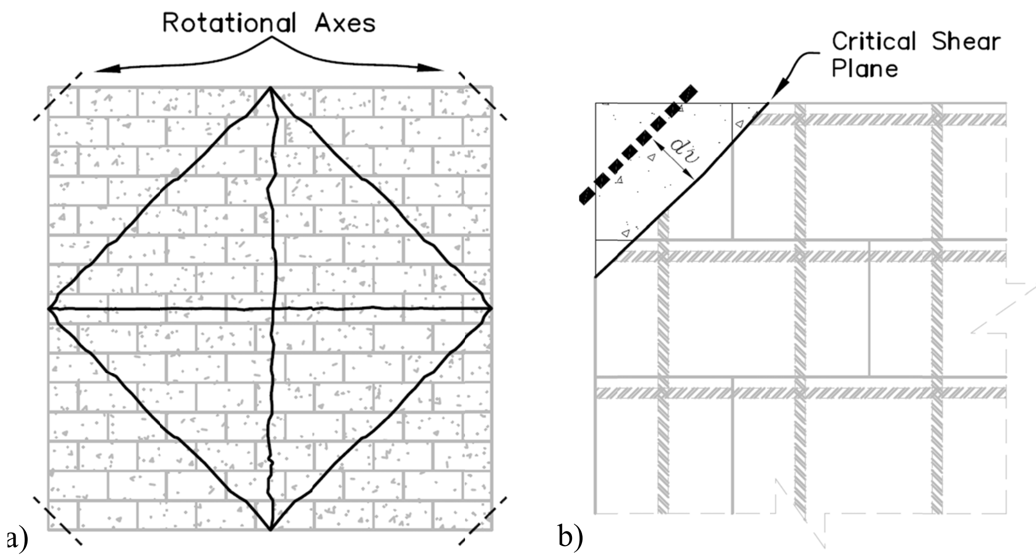

Figure 3.1. Theoretical Failure Patterns: a) Flexure; b) Shear

With the wall specimens supported at the corners only, significant shear stresses are expected to develop near these locations. By treating the wall as spanning diagonally between the supports, it becomes apparent that the critical shear plane will be at a distance d_v from the support and parallel to the axis of rotation as shown in Fig. 3.1-b. For this cross section configuration, d_v is assumed to be half the wall thickness (31 mm), indicating the wall cross sectional depth measured from the extreme compression fibre to the steel reinforcement location at the middle of the wall thickness. At this critical shear section, the shear forces are to be resisted through a combination of bond and a shear-friction mechanism across the possible shear failure surfaces (CSA 2004). As a result, the theoretical out-of-plane shear resistance V_r can be computed as:

$$V_r = CA_e + \mu A_{sv} f_{sc} \quad (3.5)$$

where C is the masonry bond resistance; A_e is the effective area of the shear plane; A_{sv} is the area of longitudinal steel passing through the shear plane; f_{sc} is the clamping stress in the steel; and μ is the coefficient of friction, taken as 1.0 (CSA 2004).

To establish an approximate wall shear capacity, the total shear capacity at the wall supports is equated with the demand resulting from an applied surface pressure. Comparing the computed values for the shear and flexural capacities, Table 3.2 shows that the wall shear capacities are significantly larger than their flexural capacities, and thus indicating that flexure would govern the wall failure mode under static loading. These theoretical capacity predictions are compared with the wall experimental static test results as described next.

Table 3.2. Static Wall Capacities

Wall	Reinf. Ratio	*Flexure*			*Shear*	
		Theoretical Capacity (kPa)	Experimental Capacity (kPa)	Diff.	Theoretical Force (kN)	Equivalent Load Capacity (kPa)
WNL	0.32%	43.7	50.7	16%	39.8	159.2
WNM	0.59%	74.2	81.9	10%	44.9	179.6
WNH	1.07%	98.9	105.0	6%	53.5	214.0

3.3.2 Test Setup

To determine the static capacities as well as correlate damage patterns for each reinforcement level, three walls were constructed concurrently and with the same materials as those used in the wall field blast testing study. The walls are labeled to reflect their reinforcement levels (***L***ow, ***M***oderate and ***H***igh), where WNL represents the wall with a D4 reinforcing bar in every-other vertical cell and horizontal course while WNM and WNH represent the walls fully reinforced with D4 (area = 25 mm^2) or D7 (area = 45 mm^2) bars in every vertical cell and horizontal course, respectively. To best replicate the field blast testing boundary conditions, the wall specimens were fit into the same test frame (bunker) used during the blast testing and linear displacement potentiometers positioned in the same quarter-grid pattern were used to capture deflections as shown in Fig. 3.2-a. To apply a uniform pressure over the surface of the specimens, an airbag with square dimensions measuring 935 mm was affixed between the wall and a rigid self-reacting support frame as depicted in Fig. 3.2-b and Fig. 3.2-c.

a) b) c)

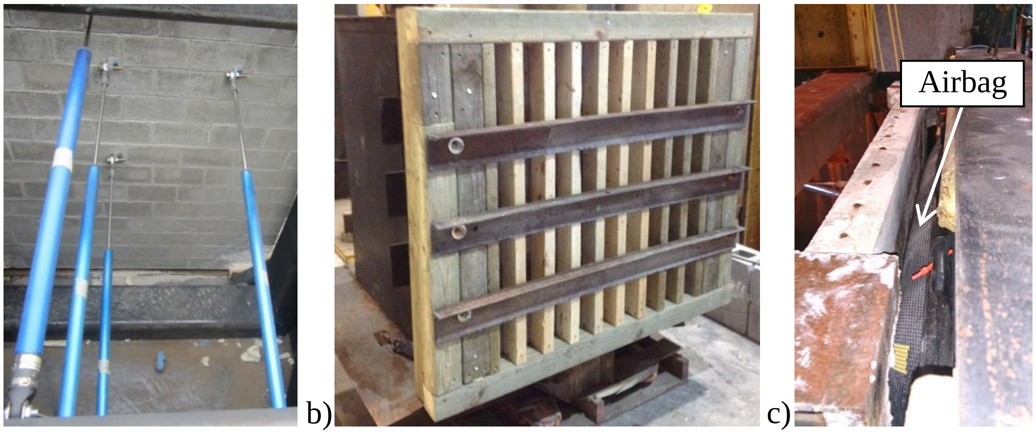

Figure 3.2. Static Test Setup: a) LVDTs; b) Reaction Frame; c) Airbag

3.3.3 Test Results

When relating the static test crack patterns in Fig. 3.3 to the theoretical flexure yield lines previously presented in Fig. 3.1-a, it can be observed that they display similar trends. Although the field blast testing of identical walls (Smith et al. 2014) resulted in more extensive cracks, the general shape and more importantly the critical failure locations match well with the theoretical expectations. In addition, there was no evidence of shear damage near the wall support locations, confirming that the static shear resistance exceeded the wall flexural strength as the theoretical analysis had predicted. The peak experimental static pressure values reached by each of the three test walls are presented in Table 3.2 along with their theoretical capacity as determined above, showing that the yield line approach presents a conservative prediction of the static two-way flexural response of the RM walls.

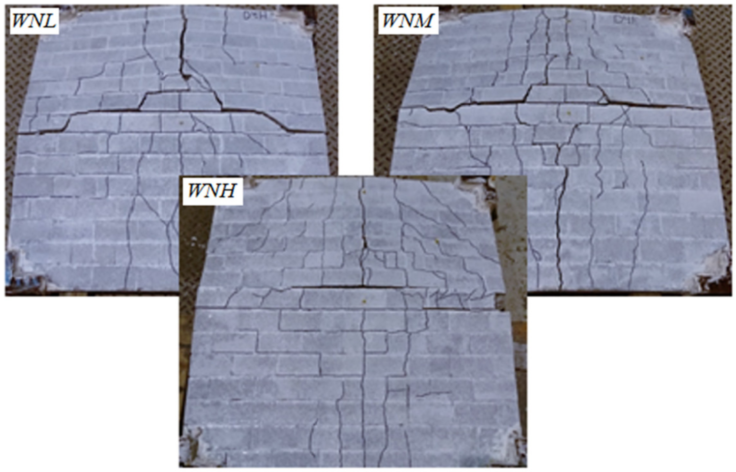

Figure 3.3. Static Testing Damage Patterns

The deflection response was captured for each wall in order to establish a comprehensive pressure-displacement function at the location of each displacement potentiometer. For comparative purposes, the mid-point displacement functions for each of the wall types are depicted in Fig. 3.4. When considering the specimens with low and moderate reinforcement ratios (WNL and WNM), it is apparent that after the ultimate capacity is reached, the specimens exhibit a ductile type response allowing for plastic strain development in the longitudinal reinforcement. In comparison, the specimen with the higher reinforcement ratio (WNH), reached its ultimate capacity and then failed in a brittle manner commonly observed in members exceeding a balanced cross section reinforcement ratio as corroborated through the theoretical calculations.

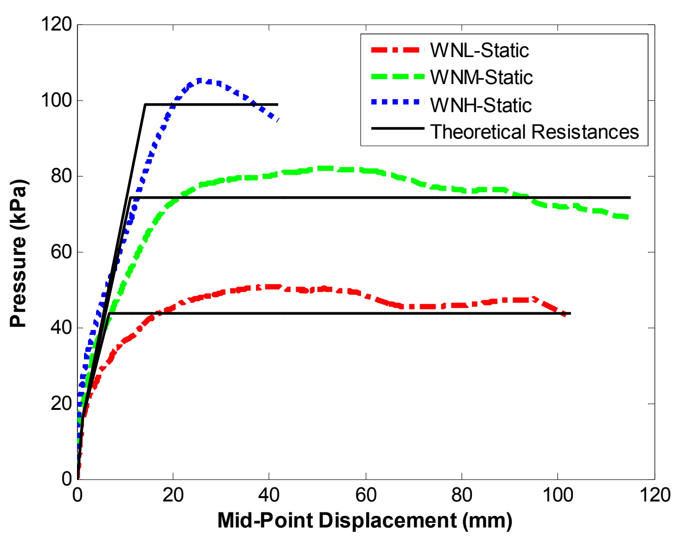

Figure 3.4. Mid-Point Resistance Functions

3.4 SDOF Model Development

3.4.1 Equation of Motion Formulation

To approximate the dynamic response of the walls to the blast loads, the complex characteristics are simplified to an equivalent spring-mass (SDOF) system. As the parameter of greatest interest is the displacement at the centre (mid-point) of the wall, all equivalent parameters are referenced to this point, with the displacement of the equivalent system equal to the mid-point displacement of the actual wall. Equivalency factors for the mass (K_M), resistance (K_R) and load (K_L) are established in order to relate the generalized characteristics of the model to the characteristics of the actual wall by equating the external work, strain energies and kinetic energies of the two systems (Baker et. al 1983; Biggs 1964). The equation of motion for the equivalent SDOF system can be expressed as:

$$K_{LM}M\ddot{u}(t) + R(u(t), t) = P(t) \tag{3.6}$$

where *M, R* and *P* are the mass, resistive and applied forces of the SDOF model and K_{LM} is the load-mass factor expressed by:

$$K_{LM} = \frac{K_M}{K_L} = \left(\frac{m \iint_A \emptyset_{x,y}^2 dA}{p \iint_A \emptyset_{x,y} dA}\right)\left(\frac{p \iint_A dA}{m \iint_A dA}\right) = \frac{\iint_A \emptyset_{x,y}^2 dA}{\iint_A \emptyset_{x,y} dA} \tag{3.7}$$

with m, p and r representing the uniform mass, applied blast pressure and resistance per unit area, respectively, and $\emptyset_{x,y}$ is the first mode shape of the two-way specimen. As mentioned earlier, the contribution of damping to the system response is neglected in this study as the peak blast response typically occurs within the first cycle (Biggs 1964).

3.4.2 Load-Mass Factors

To calculate the load-mass factors, the system response is effectively divided into three ranges: elastic, elasto-plastic, and plastic as depicted in Fig. 3.5. In this study, the elastic range is defined as the wall response up to the theoretical cracking load, determined through calculation of the theoretical cracking moment. The elasto-plastic range is considered to be bounded by the cracking load and 80% of the peak capacity, whereas the plastic range comprises the remainder of the response beyond this point. By tracking the deflection behaviour from the static tests, it was determined that development of a fully plastic response was well represented at 80% of the peak capacity.

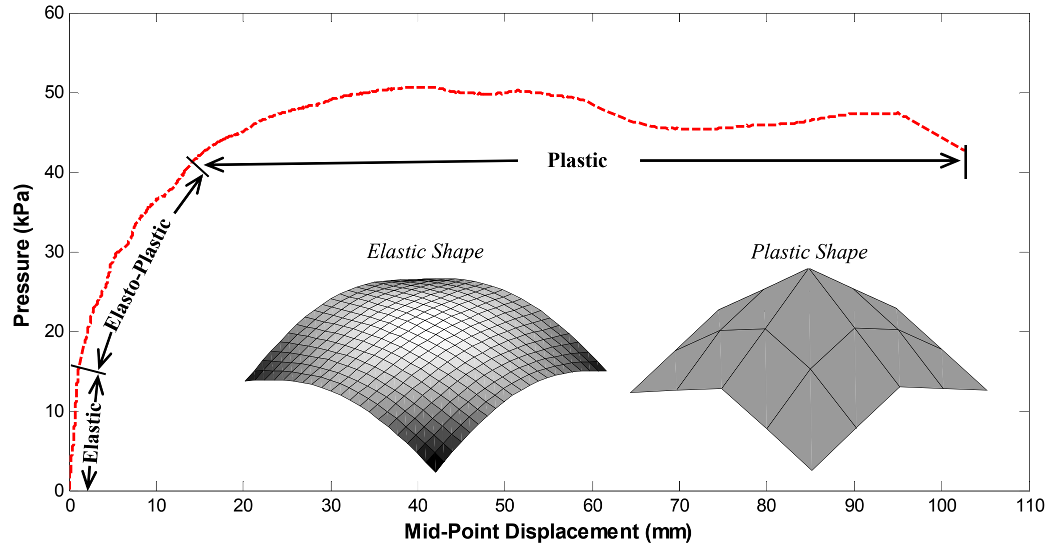

Figure 3.5. Resistance Function Strain Ranges

An appropriate mode shape for the elastic response was chosen considering the bi-harmonic deflection function established for an elastic plate supported at its corners (Lee and Ballesteros 1960) taking the un-normalized form:

$$\begin{aligned}\emptyset_{x,y}^{E} &= 22 - 12v - 2v^2 \\ &\quad + 2(-5 + 4v + v^2)\left[\frac{x^2 + y^2}{a^2}\right] \\ &\quad + (2 + v - v^2)\left[\frac{x^4 + y^4}{a^4}\right] - 6(1 + v)\left[\frac{x^2 y^2}{a^4}\right]\end{aligned} \tag{3.8}$$

where v is the poissons ratio; a is half the one-sided dimension of the wall; and x and y are the coordinates at any point with respect to the center of the wall. Through comparison with the deflection profiles measured during the static testing, this mode shape is considered to accurately represent the wall deflection response. The plastic mode shape was assumed to follow the theoretical yield line pattern previously shown by Fig. 3.1-a. Visual representations of the elastic and plastic mode shapes are depicted in the inserts of Fig. 3.5. As a result of the analysis, the corresponding load-mass factors for the elastic and plastic ranges were calculated to be 0.772 and 0.589, respectively. Within the elasto-plastic range, a linear interpolation of these two parameters was applied.

3.4.3 Resistance Functions

Since the response of the equivalent SDOF model is directly correlated to the mid-point of the wall, the resistance can be obtained directly from the corresponding pressure-displacement functions based on the static testing. To validate the accuracy of the static test results, theoretical resistance functions were developed based on a tri-linear stiffness model with stages selected to represent significant changes in the response (i.e. cracking and ultimate loads). The first stage encompasses the loads prior to the occurrence of cracking in which the gross second moment of area is calculated by:

$$I_g = \frac{1}{12} L {t_w}^3 \tag{3.9}$$

where L is the length of the wall; and t_w is the total wall thickness. The second stage, which encompasses the region between the theoretical cracking and ultimate load, is based on an average of the gross and fully cracked sections, expressed as:

$$I_{avg} = \frac{I_g + I_{cr}}{2} \tag{3.10}$$

where the fully cracked section is determined as;

$$I_{cr} = \frac{1}{3} L t_{cr}^3 + n A_s (d - t_{cr}) \tag{3.11}$$

where t_{cr} is the distance between the extreme compression fibre and the cracked neutral axis; n is the modular ratio between steel and masonry; A_s is the area of reinforcing steel; and d is the distance between the extreme compression fibre and the centroid of the reinforcement. After the theoretical capacity is reached, the third stage of the wall response assumes the development of a fully plastic mechanism until failure. The theoretical deflections are calculated using an approximate solution for an elastic plate supported only at its corners (Lee and

Ballesteros 1960) and accounting for the unique stiffness of each stage, expressed by the following equation:

$$w_{0,0} = \frac{qa^4}{48(1-v^2)D}[22 - 12v - 2v^2] \tag{3.12}$$

given;

$$D = \frac{E\, I_{g,avg}}{L(1-v^2)} \tag{3.13}$$

where *q* is the uniformly distributed pressure; and *D* is the wall flexural rigidity, which is a function of the stiffness, *EI*, depending on the strain interval. The theoretical tri-linear resistance functions were previously shown in Fig. 3.4 along with the experimental non-linear resistance functions captured during the static tests. The validity of these theoretical functions will be evaluated by comparing their response with the non-linear results as well as the captured response from the field blast testing study.

3.4.4 Pressure-Time Histories

In an attempt to best replicate the experimental blast events, the load inputs were developed from a Modified Friedlander fit (Baker et al. 1983) of the measured pressure-time history for each blast test (Smith et al. 2014). It was necessary that the modelling load parameters accurately reflect the experimental values to allow for direct comparison between the wall responses under the corresponding charge weights and reinforcement levels. To evaluate the validity of the measured pressure histories, predicted parameters based on the experimental charge weights (*W*) and standoff distances (*R*) were developed using the blast load parameter calculation program ConWep (Hyde 1990) and subsequently used in the SDOF model. Table 3.3 presents the pressure-time history parameters for each load with the charge weights appended to the wall type labels for easy identification. In most cases, the difference between the pressure and impulse of the respective loads is less than 10%, with the exception of wall type WNH-12, where the measured impulse was lower than the others captured at the same scaled-distance and 23% lower than the predicted value. The field blast testing had also included tests completed at a smaller scaled-distance (Z=1.61 m/kg$^{1/3}$) than reported in this study. Due to the significant level of shear damage resulting from this large DBT level, attempting to model the response using these flexure-based resistance functions was deemed to be inaccurate and was not considered as part of this study which aimed to model the flexural response only.

Table 3.3. Pressure Input Matrix

Wall	Scaled Distance Z ($m/kg^{1/3}$)	*Measured Load Parameters*			*Predicted Load Parameters*		
		P^+ (kPa)	I^+ (kPa.ms)	t_d (ms)	P^+ (kPa)	I^+ (kPa.ms)	t_d (ms)
WNL-6	2.75	460	489	3.23	417	450	4.70
WNM-6	2.75	405	466	3.15	417	450	4.70
WNH-6	2.75	343	402	2.97	417	450	4.70
WNL-12	2.18	698	628	3.22	810	747	4.81
WNM-12	2.18	871	702	2.28	810	747	4.81
WNH-12	2.18	780	581	1.87	810	747	4.81

P^+, I^+ and t_d represent the peak pressure, specific impulse and duration of the positive phase

3.4.5 Dynamic Reactions

The development of shear stresses throughout the time-history analysis of the wall responses was monitored to ensure that the wall shear capacity was not exceeded throughout the flexural response history. Due to the geometry and boundary conditions, which approximates the reactions as a point load at each corner, the critical (maximum) shear stress develops near the supports, proportional to the dynamic reaction force. The dynamic reactions are calculated by equilibrating the dynamic forces on the wall as shown in Fig. 3.6 and are dependent on the combined effects of the inertial force and the applied load (Biggs 1964). The dynamic equilibrium is a function of the support reaction, $V(t)$, the total inertial force, $I_{xyz}(t)$, and the applied blast pressure, $P(t)$, over the wall area, A_r. Since the inertial forces are assumed to follow the same distribution as the deflected shape (Biggs 1964), the force equilibrium is expressed as:

$$4V(t) + I_{xyz}(t) - P(t)A_r = 0 \qquad (3.14)$$

where;

$$I_{xyz} = \rho_{x,y} t_w \ddot{u}(t) \iint_A \emptyset_{x,y} dA \qquad (3.15)$$

with $\rho_{x,y}$ being the wall density; t_w as the wall thickness; $\ddot{u}(t)$ as the acceleration at the centre; and $\emptyset_{x,y}$ as the deflected (mode) shape. As such, the reaction forces can be calculated by tracking the system accelerations of the equivalent SDOF model throughout the response history.

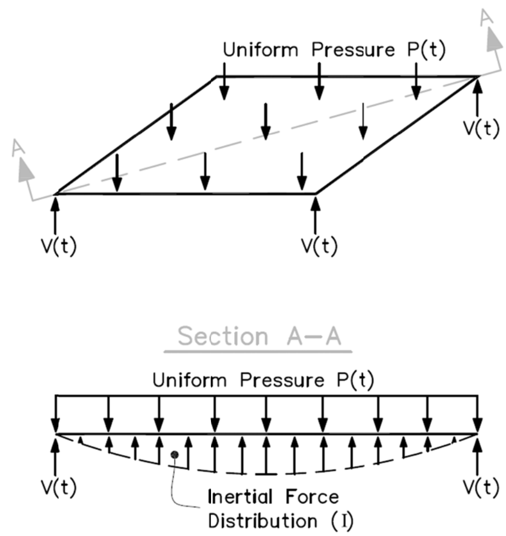

Figure 3.6. Dynamic Equilibrium

3.5 SDOF Model Results and Discussion

3.5.1 Peak Response Predictions

The non-linear resistance functions obtained through static testing were used to initially predict the peak displacement at the mid-point of the walls. Due to differences in the measured and predicted pressure parameters, the SDOF model was used to calculate the response using both values to evaluate the validity of the measured pressure-time histories. Fig. 3.7 depicts a sample of the modelled responses for both the measured and predicted loads along with the actual wall mid-point displacement history from the experimental blast testing. The results of each model generally follow the same shape of the experimental response with an almost simultaneous occurrence of the maximum response values.

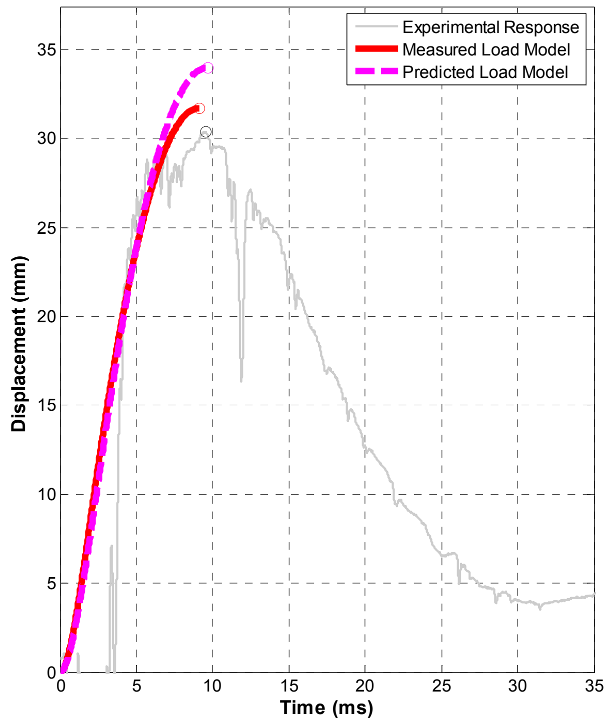

Figure 3.7. Sample Model Response (WNM-12)

The non-linear resistance functions were replaced with the theoretical functions and the SDOF model was again used to determine the response history and ultimately the peak displacement for both the measured and predicted loads. Table 3.4 presents the peak responses of both load inputs for the theoretical (piece-wise linear) and experimental (non-linear) resistance functions to allow for a direct comparison with the displacements from the field blast testing. The results are also shown graphically in Fig. 3.8 where it can be seen that the peak response of each resistance function differs by less than 10%. This observation shows that the non-linear experimental resistance function and in turn the actual wall response, is well represented by the theoretical piece-wise linear model. Through comparison of the different load responses, Fig. 3.8 also shows that, on average, the measured blast load typically results in a more accurate peak displacement considering the uncertainty that typically arises in blast testing. There is a discrepancy in the WNH wall type subjected to the smaller scaled-distance ($Z=2.18\ m/kg^{1/3}$), where the modelled peak response is more than 20% lower than that measured in the field blast testing. This error may be attributed to the pressure transducer measurements since the load parameters of this test, in particular the specific impulse, were significantly lower than those measured (as well as those predicted) at the same threat level, as was previously discussed. In this case, the peak response from the predicted load is considered to be more representative of the actual wall response for the WNH-12 wall.

Table 3.4. Peak Mid-Point Displacement Results

Wall	Blast Disp. (mm)	*Experimental Resistance*				*Theoretical Resistance*			
		Measured Load (mm)	$\frac{\Delta}{\Delta_b}$	Predicted Load (mm)	$\frac{\Delta}{\Delta_b}$	Measured Load (mm)	$\frac{\Delta}{\Delta_b}$	Predicted Load (mm)	$\frac{\Delta}{\Delta_b}$
WNL-6	18.2	24.9	*1.37*	21.6	*1.19*	23.7	*1.30*	20.0	*1.10*
WNM-6	13.7	17.8	*1.30*	16.7	*1.22*	16.2	*1.18*	15.2	*1.11*
WNH-6	12.8	13.1	*1.02*	14.4	*1.13*	13.1	*1.02*	14.4	*1.13*
WNL-12	31.5	37.0	*1.17*	48.7	*1.55*	38.1	*1.21*	52.4	*1.66*
WNM-12	30.4	31.7	*1.04*	34.0	*1.12*	30.6	*1.01*	33.2	*1.09*
WNH-12	26.1	20.6	*0.79*	27.8	*1.07*	19.9	*0.76*	27.6	*1.06*

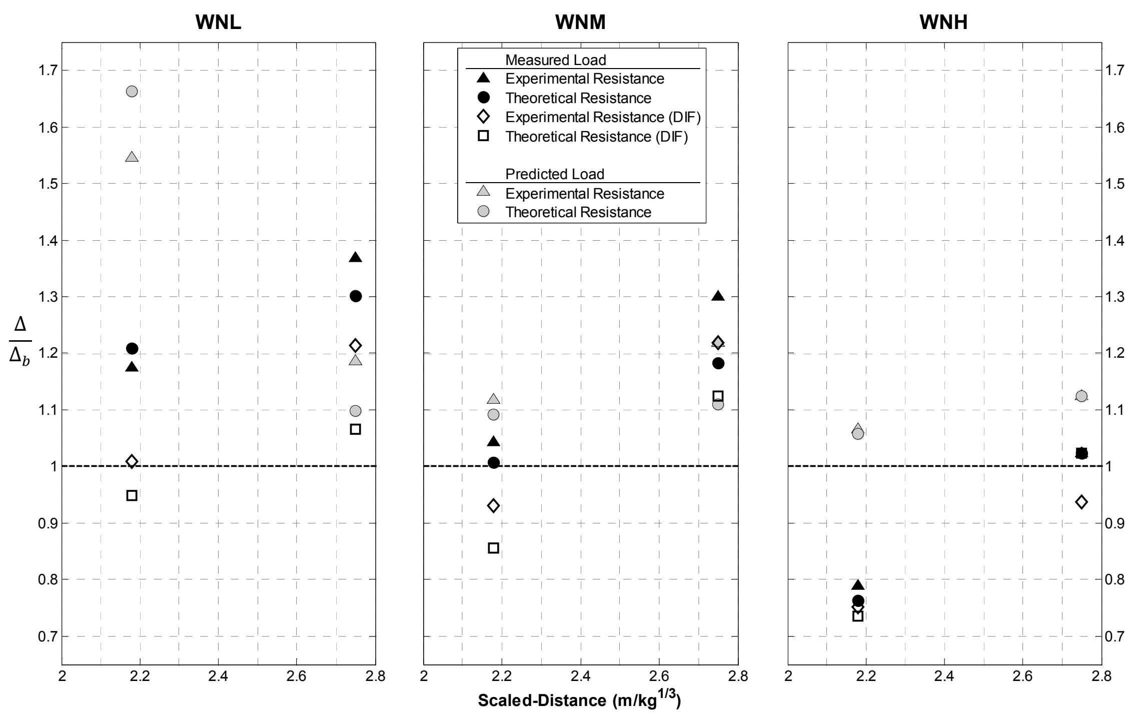

**Note: DIF refers to the inclusion of the dynamic strength effects.*

Figure 3.8. Comparison of Model Responses (Normalized by Field Blast Tests)

3.5.2 Strain-Rate Dependent Strengths

By observing both Table 3.4 and Fig. 3.8, the measured load overestimates the peak response by as much as 37% using resistance functions based on static tests only. These results can be attributed to ignoring the implications of highly impulsive loads on material mechanical properties. Extremely rapid strain rates, common in blast loading, often result in a notable increase in material capacities. To account for this, blast standards (ASCE 2011; CSA 2012) outline strength increase factors based on the probabilistic strain rates of an explosive event. Due to the threat levels of the experimental program being classified as far-range, strain-rates can be estimated as 1 mm/mm/second (U.S. Department of the Army 2008). The dynamic strength, S_d, is a function of the static strength, S_s, multiplied by a strength increase factor, *SIF,* and a dynamic increase factor, *DIF*. In this study, the *SIF* and *DIF* are equal to 1.1 and 1.2 respectively for both the concrete masonry and reinforcing steel parameters under flexure (ASCE 2011; CSA 2012).

Using these factors to calculate new theoretical capacities (including strain rate effects) based on yield line analysis allows for the determination of an overall wall capacity increase factor, to be used as an adjustment for the entire wall resistance function. The calculated capacity increase factors of 1.32, 1.32 and 1.26 result in strain-dependent theoretical capacities of approximately 67 kPa, 108 kPa and 132 kPa for the WNL, WNM and WNH wall types, respectively. The discrepancy in the capacity increase factor for the WNH wall type arises as a result of the specimen cross section exceeding its balanced reinforcement ratio. Subsequently, as the steel bars did not develop yield, both the *SIF* and *DIF* were kept at unity. To show the implications of accounting for the capacity increase effects on the wall peak response values, the modelled values for the measured loads were added to Fig. 3.8, which had previously shown the peak results obtained from the original experimental and theoretical resistance functions. In several cases, incorporating the dynamic effects resulted in the modelled responses being considerably closer to those obtained during the field blast testing than when they are neglected. This shows the significance of the dynamic material properties and how, by taking advantage of them, design requirements can be reduced while still achieving a desirable performance limit.

3.5.3 Dynamic Reactions and Shear Forces

As the resistance functions are based entirely on flexural results and properties, it was necessary to track the development of shear forces throughout the response to ensure that shear failure did not govern the wall damage mode. Table 3.5 outlines the static and dynamic theoretical shear capacities, the peak dynamic reactions for the models subjected to both the measured and predicted loads, and finally the peak shear force required to be resisted. The dynamic shear capacities include strength (*SIF*) and dynamic (*DIF*) increase factors, both equal to 1.1 under direct shear (ASCE 2011; CSA 2012).

Table 3.5. Shear Capacities, Dynamic Reactions and Shear Demands

Wall	*Shear Capacity (kN)*		*Peak Reaction (kN)*		*Peak Shear Force (kN)*	
	Static	Dynamic	Measured Load	Predicted Load	Measured Load	Predicted Load
WNL-6	39.8	48.2	41.5	34.3	34.4	28.5
WNL-12	39.8	48.2	55	57.5	45.7	47.7
WNM-6	44.9	54.3	44.6	36.8	37.0	30.5
WNM-12	44.9	54.3	77.5	60.4	64.3	50.1
WNH-6	53.5	64.7	43.8	38.1	36.4	31.6
WNH-12	53.5	64.7	81.7	61.9	67.8	51.4

Through comparison of the shear demand and corresponding wall capacity, it is seen that at the larger scaled-distance, corresponding to a lower DBT level, the wall capacity far exceeds the shear demand. This is corroborated by the field blast tests (Smith et. al 2014) showing no signs of shear damage at these blast load levels. At the smaller scaled-distance (larger threat level) the only wall in which the shear demand significantly surpasses the capacity is in the WNM-12 wall type when modelled using the experimental load. It is of importance to note that, during the field blast testing (Smith et. al 2014), WNM-12 was the only wall reported in Table 3.5 that exhibited signs of shear damage despite being dominated by a flexural action. Signs of shear damage were expected as the increased DBT level resulted in a higher impulsive loading condition, where the contribution of shear action is increased as previously discussed. It should be noted that there is typically a significant level of performance uncertainty due to both the assumptions involved in the theoretical shear capacity calculations as well as the uncertainty in the load application being the measured or predicted.

Nonetheless, the overall results and observations aid in showing the validity of using the flexural resistance function to simulate the response of the blast testing at the considered threat levels.

3.6 Infill Wall Performance Charts (P-I Diagrams)

To aid in the design and analysis of any component subjected to blast loads, the American (ASCE 2011) and Canadian (CSA 2012) blast standards allow for the use of performance charts, typically expressed by combinations of pressure and impulse, to estimate the peak response and subsequent damage level of different structural components. Currently, the standards include and refer to the same performance chart regardless of the material, amount of reinforcement, boundary configurations and response behaviour (flexure/shear), making them inaccurate for specific component screening or preliminary analysis and design.

To show the influence of changing only the reinforcement ratio, P-I diagrams were used from a code developed by Campidelli (2014) for full-scale wall specimens, based on the theoretical resistance functions and incorporating the dynamic strain-rate effects. Due to the mode shape considered, the P-I diagram shows the flexural response only. The reinforcement ratios presented correspond to a 15M bar in every other vertical cell and horizontal course (0.32%), a 15M bar in every vertical cell and horizontal course (0.59%), and finally a 25M bar in every vertical cell and horizontal course (1.32%). The performance limits outlined in the current blast standards are defined as: the initiation of yielding in the reinforcement ($\mu=1$) or the support (chord) rotations reaching values of 2, 8 or 15 degrees, and relate to prescribed damage levels of *Superficial*, *Moderate*, *Heavy* and *Blowout*, respectively (ASCE 2011; CSA 2012). The iso-damage curves illustrated in Fig. 3.9 show the sensitivity of the results, where the ratio between the pressure at the highest reinforcement ratio (1.32%) and the smallest (0.32%) was over 2.0 for each performance limit. In addition, the ratios for the impulse values were over 1.4 for the rotation limits and 2.0 for the yielding limit when compared at the aforementioned reinforcement ratios.

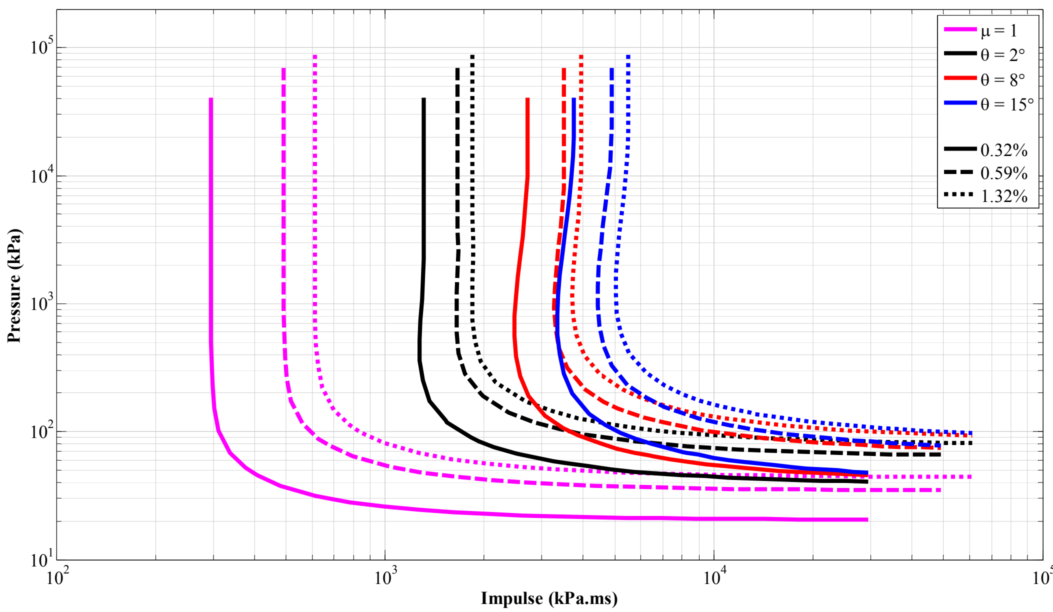

Figure 3.9. Full-Scale Infill Wall Performance Chart (P-I Diagram)

3.7 Implication of Support Conditions on Response

To understand the influence of the studied support conditions on the peak response, common boundary conditions were investigated by repeating the SDOF analysis using theoretically derived resistance functions, including the dynamic strain-rate effects, and the measured loads. As the tested walls were supported in such a way as to allow unrestrained rotation about their corners, it was expected that the peak mid-point response would be bounded between configurations inducing complete one-way and two-way behaviour. By supporting the top and bottom edges of the walls in a simply supported (rotationally unrestrained) manner, a one-way response is developed and resisted by only the reinforcement in the vertical direction, which would produce a larger response and hence an upper bound. Alternatively, supporting the walls on all four sides induces a two-way response, which by restraining the displacements along all edges, would result in a smaller mid-point response and hence act as a lower bound. The theoretical resistance functions for each of these bounding configurations were developed based on an elastic perfectly-plastic model using parameters derived by Biggs (1964) as presented in Table 3.6. It is important to note that, even before comparing the system responses, the presented parameters in the table bound those of the model used for the infill walls.

Table 3.6. Support Condition Model Parameters (Biggs 1964)

Support Conditions	K_{LM} Elastic	K_{LM} Plastic	W_{fl}
Current Model	0.772	0.589	$16M_u/L^2$
One-Way Simple	0.780	0.660	$8M_u/L^2$
Two-Way Simple	0.670	0.510	$24M_u/L^2$

Results for the peak mid-point displacements are presented in Table 3.7 for the investigated bounds normalized by the results of the modelled infill walls. Similar to the model parameters, the responses of the infill walls with the selected boundary conditions fall between these upper and lower bounds. Although a numerical relationship cannot be drawn between the experimental results and the respective bounds, this shows that despite the response complexity of infill walls, the expected response can be rationalized as being within these two well defined boundary conditions.

Table 3.7. Bounded Support Displacements (Normalized by Modelled Walls, Δ_m)

Wall	Two-Way Simple, $\frac{\Delta}{\Delta_m}$	Modelled Infill	One-Way Simple, $\frac{\Delta}{\Delta_m}$
WNL-6	0.69	1	1.90
WNM-6	0.51	1	1.41
WNH-6	0.45	1	1.11
WNL-12	0.80	1	2.15
WNM-12	0.67	1	1.81
WNH-12	0.55	1	1.43

To investigate the bounding support conditions at threat levels outside those considered within the experimental program, Fig. 3.10 depicts the P-I diagrams generated for the modelled full-scale infill walls, identical to Fig. 3.9, as well as the two hypothesized bounds. It is obvious that at all combinations of pressure and impulse, the response of the modelled infill walls is bounded between one-way and two-way simply supported conditions. Changes in the pressure and impulse values depending on the level of reinforcement are consistent with those discussed previously along with Fig. 3.9, where the respective ratios for pressures and impulses related to the support (chord) rotation limits were over 2.0 and 1.4 when comparing the largest reinforcement ratio (WNH) to lowest (WNL).

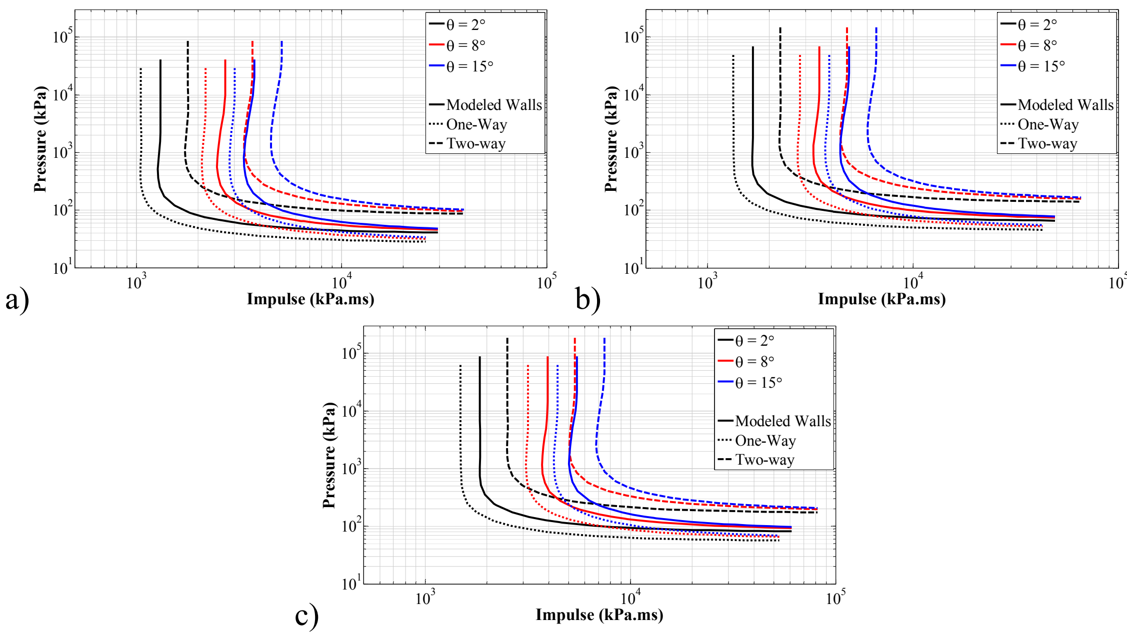

Figure 3.10. Full-Scale P-I Diagrams with Bounding Support Conditions: a) WNL; b) WNM; c) WNH

3.8 Conclusions

The accuracy of modelling the dynamic out-of-plane behaviour due to blast loading of non-integral, reinforced masonry infill walls was investigated through comparison of modelled responses with those obtained through experimental blast testing. Single Degree of Freedom (SDOF) models were used with resistance functions representing each of the three unique reinforcement ratios (**L**ow, **M**oderate and **H**igh) and pressure-time histories both measured during experimental testing and derived from predicted parameters at design-basis threat (DBT) levels of $2.75\ m/kg^{1/3}$ and $2.18\ m/kg^{1/3}$. After validating the experimental results at these DBT levels, the models were used to develop performance charts which estimate the flexural response only at threat levels outside of the experimental scope and draw conclusions about the implications of the level of reinforcement.

By comparing the peak response values for each resistance function, it was shown that the theoretically derived resistance function could replicate the response of the non-linear resistance function with over 90% accuracy. It was also shown that for all cases, not accounting for strength increases due to the material strain-rate effects resulted in a significant over-prediction of the peak response. By incorporating the strength increase factors prescribed by the current blast standards (ASCE 2011; CSA 2012), these over-predictions were reduced from a maximum of 37% to 22% and in some cases almost matching the experimental peak response.

Current code practices (ASCE 2011 and CSA 2012) allow for the use of performance charts to estimate the peak response of components. Unfortunately, these performance charts make no account of material, level of reinforcement or boundary configuration. To investigate their validity in terms of reinforced masonry, full-scale pressure-impulse (P-I) diagrams were developed based on the code prescribed performance limits for the flexural response only. These diagrams show that by changing only the reinforcement levels, pressure and impulse values could increase by over two-fold for the same level of performance.

Due to the complex and ill-defined support conditions that traditional non-integral and non-participating infill walls present, common boundary conditions were modelled in an attempt to better understand and bound the response. By repeating the SDOF analysis using theoretically derived resistance functions for one- and two-way simply supported walls having the same level of reinforcement, it was shown that the peak response of the modelled infill walls are bounded by these conditions at the threat levels presented by the experimental program. To investigate these bounds at all threat levels, full-scale P-I diagrams were developed for the boundary conditions and compared with the modelled infill walls at all reinforcement ratios separately. By doing this it was shown that, regardless of the threat level and reinforcement ratio, these two well-defined support conditions bound the complex response of the modelled infill walls investigated.

This study shows that not only can simplified SDOF models be used to validate flexure-dominated experimental results and predict peak flexural responses when testing is unavailable, but they can also be readily used in the development of performance limits and corresponding charts for a variety of assemblage configurations. The results and subsequent analysis of the study should be considered in future modifications to the current performance limits of the blast standards.

3.9 Notation for Chapter 3

The following symbols are used in this paper:

a	=	half the one-side dimension of specimen;
A_e	=	effective area of shear surface;
A_f	=	surface area of full-scale SDOF model;
A_r	=	surface area of reduced-scale SDOF model;
A_s	=	area of longitudinal reinforcement within cross section;
A_{sv}	=	area of longitudinal reinforcement passing through shear plane;
C	=	cohesive force of masonry interface;
d	=	distance from extreme compression fibre to reinforcement centroid;
D	=	flexural rigidity of elastic plate;
DIF	=	dynamic increase factor;
d_v	=	distance from support to critical shear plane;
E	=	elastic modulus;
f_{sc}	=	clamping stress in longitudinal steel;
I^+	=	positive specific impulse of blast;
I_{avg}	=	average second moment of area;
I_{cr}	=	cracked section second moment of area;
I_g	=	gross section second moment of area;
$I_{xyz}(t)$	=	inertial force;
K_L	=	dynamic load factor;
K_{LM}	=	dynamic load-mass factor;
K_M	=	dynamic mass factor;
K_R	=	dynamic resistance factor;
L	=	one-sided dimension of specimen;
m	=	actual mass of reduced-scale wall;
M_f	=	mass of full-scale SDOF model;
M_r	=	mass of reduced-scale SDOF model;
M_u	=	section ultimate moment resistance;
n	=	modular ratio between elastic moduli of steel and masonry;
p	=	applied blast pressure per unit area;
$P(t)$	=	applied blast force;
P_o	=	peak reflected blast pressure;
q	=	uniform surface pressure
R	=	standoff distance;
$R(u(t))$	=	displacement dependent system resistance;
S_d	=	dynamic material strength;

SIF	=	strength increase factor;
S_s	=	static material strength;
t_w	=	specimen thickness;
t_{cr}	=	distance from extreme compression fibre to cracked neutral axis;
t_d	=	positive phase duration;
$u_f(t)$	=	displacement of full-scale SDOF model;
$u_r(t)$	=	displacement of reduced-scale SDOF model;
$\ddot{u_f}(t)$	=	acceleration of full-scale SDOF model;
$\ddot{u_r}(t)$	=	acceleration of reduced-scale SDOF model;
v	=	poisson ratio of wall specimen;
$V(t)$	=	dynamic reaction;
V_r	=	theoretical shear resistance;
$w_{0,0}$	=	elastic displacement at center of plate;
W	=	charge weight;
W_{fl}	=	theoretical flexural capacity;
Z	=	scaled-distance;
λ	=	scale factor;
μ	=	friction coefficient;
ρ_{xy}	=	mass per unit area of wall;
$\emptyset_{x,y}$	=	deflected shape of wall;
$\emptyset_{x,y}^{E}$	=	two-way mode shape of elastic plate;

3.10 References for Chapter 3

Abou-Zeid, B. M., El-Dakhakhni, W. W., Razaqpur, A. G., and Foo, S. (2011). "Response of arching unreinforced concrete masonry walls to blast loading." *J. Struct. Eng.*, 137(10), 1205-1214.

American Society of Civil Engineers (ASCE). (2011). "Blast protection of buildings." *ASCE 59-11*, Reston, VA.

Baker, W. E., Cox, P. A., Westine, P. S., Kulesz, J. J., and Strehlow, R. A. (1983). "Explosion hazard and evaluation", Elsevier, Amsterdam.

Baker, W. E., Westine, P. S., and Dodge, F.T. (1973). "Similarity methods in engineering dynamics: theory and practice of scaled modeling", Rochelle Park, NJ.

Baylot, J. T., Bullock, B., Siawson, T. R., and Woodson, S. C. (2005). "Blast response of lightly attached concrete masonry unit walls." *J. Struct. Eng.*, 131(8), 1186–1193.

Biggs, J.M. (1964). "Introduction to structural dynamics", Toronto, ON, Canada.

Campidelli, M. (2014). "Matlab code to develop P-I diagrams." Provided through personal communication.

Canadian Standards Association (CSA). (2004). "Design of masonry structures." *CSA S304.1-04*, Mississauga, ON, Canada.

Canadian Standards Association (CSA). (2012). "Design and assessment of buildings subjected to blast loads." *CSA S850-12*, Mississauga, ON, Canada.

Dennis, S. T., Baylot, J. T., and Woodson, S. C. (2002). "Response of ¼-scale concrete masonry unit (CMU) walls to blast." *J. Eng. Mech.*, 128(2) 134-142.

Fujikura, S. and Bruneau, M. (2011). "Experimental investigation of seismically resistant bridge piers under blast loading." *J. Bridge Eng.*, 16(1), 63-71.

Harris, H. G., and Sabnis, G. M. (1999). "Structural modeling and experimental techniques", 2nd Ed., CRC Press, Boca Raton, FL.

Henderson, R. C., Fricke, K. E., Jones, W. D., Beavers, J. E., and Bennett, R. M. (2003). "Summary of a large- and small-scale unreinforced masonry infill test program." *J. Struct. Eng.*, 129(12), 1667–1675.

Hopkinson, B. (1915). *British Ordinance Board Minutes 13565*.

Hyde, D. (1990). "User's guide for microcomputers programs CONWEP and FUNPRO-applications of TM 5-855-1." Experimental Station, U.S. Army Engineers Waterways, Vicksburg, MS.

Lee, S.L., and Ballesteros, P. (1960). "Uniformly loaded rectangular plate supported at the corners." *Int. J. Mech. Sci.*, 2, 206-211.

Park, R., and Gamble, W.L. (2000). "Reinforced concrete slabs." Toronto, ON, Canada.

Shi, Y., Hao, H., and Li, Z-X. (2008). "Numerical derivation of pressure-impulse diagrams for prediction of RC column damage to blast loads." *J. Impact Eng.*, 35(11) 1213-1227.

Smith, N.L., El-Dakhakhni, W.W., Tait, M.J., and Mekky, W.F. (2014). "Blast performance assessment of two-way reinforced concrete block infill walls under different design-basis threat levels." *Submitted to ASCE Journal of Structural Engineering* Mar. 10, 2014.

U.S. Department of the Army. (1986). "Fundamentals of protective design for conventional weapons." *TM 5-855, U.S. Department of the Army Technical Manual*, Washington, D.C.

U.S. Department of the Army. (1999). "Structures to resist the effects of accidental explosions." *TM 5-1300, U.S. Department of the Army Technical Manual*, Washington, D.C.

U.S. Department of the Army. (2006). "Minimum Anti-Terrorism Standards for Buildings." *UFC 4-010-01, U.S. Department of the Army Technical Manual*, Washington, D.C.

U.S. Department of the Army. (2008). "Design of structures to resist the effects of accidental explosions." *UFC 3-340-02, U.S. Department of the Army Technical Manual*, Washington, D.C.

CHAPTER 4: CONCLUSIONS AND RECOMMENDATIONS

4.1 Conclusions

This thesis investigated the out-of-plane blast performance of non-integral (i.e. no physical connection with the surrounding frame) and non- participating (i.e. not in full contact with the top and side frame members as per seismic detailing requirements) reinforced masonry (RM) infill walls through experimental blast testing and dynamic modelling. Due to the significant cost, safety concerns and site limitations on charge sizes associated with experimental blast testing, one-third scale wall specimens (λ=1/3) with dimensions of 1.0 m in length and height were constructed to replicate a 3.0 m by 3.0 m prototype using one-third scale true-replicas of the standard 190 mm concrete block units. The walls were also constructed with three unique reinforcement ratios (**L**ow, **M**oderate and **H**igh), which allowed for conclusions to be drawn upon the influence of the level of reinforcement on the response. The ill-defined boundary conditions that currently exist in infill wall applications result in the complex out-of-plane behaviour of these components. To simplify the response, the replicated walls were configured in such a way as to restrain displacements at their corners only and allow for their two-way bending with unrestrained corner rotation. The following sections summarize the conclusions already drawn within the experimental blast testing (Chapter 2) and the Single Degree of Freedom (SDOF) dynamic modelling (Chapter 3) journal articles. Following the conclusions, recommendations are made for future research as well as code applications.

4.1.1 Experimental Blast Testing

The aforementioned walls were subjected to a range of design-basis threat (DBT) levels invoked through live explosive charges. The DBT levels are measured in terms of the scaled-distance, where equivalent TNT charge sizes of 6 kg, 12 kg and 30 kg at a standoff distance of 5.0 metres resulted in scaled-distances of 2.75 m/kg$^{1/3}$, 2.18 m/kg$^{1/3}$ and 1.61 m/kg$^{1/3}$, respectively.

At the lowest DBT level (Z=2.75 m/kg$^{1/3}$) the support (chord) rotations ranged between 1.0° and 1.5° at the highest and lowest reinforcement ratios, respectively. The American (ASCE 59-11) and Canadian (CSA S850-12) blast standards prescribe these responses as *Superficial* to *Moderate* levels of damage and was qualitatively verified through visual observation of tested specimens. The walls tested under the intermediate DBT level (Z=2.18 m/kg$^{1/3}$) exhibited support (chord) rotations ranging from 2.1° to 2.6°, again at the highest and lowest reinforcement ratios. Under the performance limits of the current codes, their response is classified as being a *Heavy* damage level. Finally, the highest DBT level (Z=1.61 m/kg$^{1/3}$) resulted in wall support (chord) rotations at the highest and lowest levels of reinforcement being between 5.4° and 7.1°, respectively. As was the case with the moderate DBT level, these numerical threshold-based performance limits fall within the *Heavy* damage classification even though visual inspection of the tested specimens had shown that these walls possessed very little, if any, post-blast structural integrity. The reason for this perceived under-classification of damage levels results from the performance limits being implicitly based on flexural response without accounting for combined failure modes (e.g. shear-flexure). This study had shown that when subjected to impulsive loads, similar to their reinforced concrete (RC) counterparts, RM wall response and ultimate damage might be governed and significantly affected by combined shear-flexure response. This indicates the need to revisit current code quantitative performance threshold provisions and include more qualitative performance assessment criteria. Along with other reported studies, the current test results demonstrate the need to account for blast-specific failure modes that may neither be predicted through static testing nor mitigated through subsequent detailing.

4.1.2 Dynamic Modelling

The dynamic response of the aforementioned wall specimens was investigated through the use of SDOF modelling. Resistance functions representing each of the unique reinforcement ratios were derived based on static testing of identical specimens as well as theoretical yield line analyses. The loads applied to each model were the pressure time-histories measured during the corresponding experimental blast tests as well as estimated from predicted parameters. Due to the presence of shear damage at the largest DBT level (Z=1.61 m/kg$^{1/3}$) in the experimental blast testing, the model was only used to validate the peak response at the other two blast tested DBT levels (Z=2.18 m/kg$^{1/3}$ and Z=2.75 m/kg$^{1/3}$). This was necessary as the resistance functions, derived statically, had shown no signs and hence did not account for the shear behaviour.

By comparing the peak response values for each resistance function, it was shown that the theoretically derived resistance function could replicate the flexural response of the non-linear (experimental) resistance function with over 90% accuracy. It was also shown that for all cases, not accounting for strength increases due to the material strain-rate effects resulted in a significant over-prediction of the peak response. By incorporating the strength increase factors prescribed by both the American (ASCE 59-11) and Canadian (CSA S850-12) blast standards, these over-predictions were reduced from a maximum of 37% to 22% and in some cases almost matched the peak response captured during the experimental blast testing. This is significant when considering the level of uncertainty prevalent in blast loading.

The current blast codes allow for the use of performance charts to estimate the peak response of components. Unfortunately, these performance charts make no account of material, level of reinforcement or boundary conditions. To investigate their validity in terms of reinforced masonry, full-scale pressure-impulse (P-I) diagrams were developed for flexural response based on the code prescribed performance limits. These diagrams had shown that by changing only the reinforcement levels, pressure and impulse values could increase by over two-fold for the same level of performance.

Due to the complex and ill-defined support conditions that traditional non-integral and non-participating infill walls present, common boundary conditions were modelled in an attempt to better understand and bound the response. By repeating the SDOF analysis using theoretically derived resistance functions for one- and two-way simply supported walls having the same levels of reinforcement, it was shown the peak response of the modelled infill walls are bounded by these conditions at the DBT levels presented by the experimental program. To investigate these bounds at all threat levels, full-scale P-I diagrams were developed for the boundary conditions and compared with the modelled infill walls at all reinforcement ratios separately. By doing this it was shown that, regardless of the DBT level and reinforcement ratio, these two well-defined support conditions bound the complex response of the modelled infill walls.

This study had shown that not only can simplified SDOF models be used to validate flexure-dominated experimental results and predict peak flexural responses when testing is unavailable, but they can also be readily used in the development performance limits and corresponding charts for a variety of assemblage configurations. It is imperative that the results and subsequent analysis of the study be considered in future modifications to the current performance limits of the blast standards.

4.2 Future Research and Recommendations

Due to cost and time constraints, each level of reinforcement was tested at each DBT level only once. Although the behaviour (i.e. two-way action and combined shear-flexure) was well documented, it is imperative that the test matrix be repeated to ensure the peak-response results are statistically significant. As replica walls were tested, it is also suggested that future research initiatives include testing of the full-scale prototypes in order to validate the accuracy of using replicas as well as the inherent assumptions in the scaling techniques.

The results and accompanying analysis of this study have shown that there is an immediate need for continuing research in structural-blast response, especially for masonry components. The presence of shear damage resulting from highly impulsive DBT levels, in this study as well as reported by others, is a significant mechanism that the current flexure-based code requirements do not account for. It is imperative that studies such as these, as well as future research into this blast-shear behaviour, form the basis for modification of future *quantitative* and *qualitative* code provisions. To prevent this brittle and undesirable shear failure mechanism in construction applications, it is suggested that future detailing provisions be made in order to strengthen masonry infill walls at critical shear locations, ensuring these components develop the more desirable flexural response.

APPENDIX A – CONSTRUCTION AND TEST SETUPS

The following sections present photographs depicting the wall construction, the blast test setup and the static test setup.

A.1 Wall Construction

a) 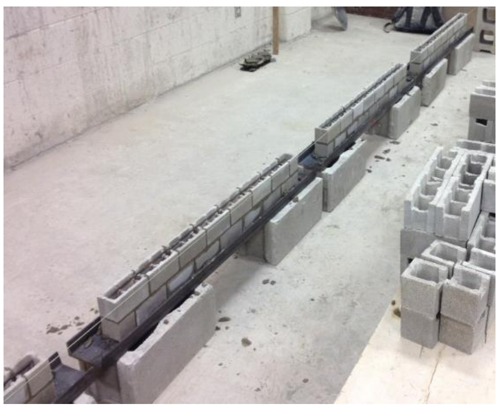 b) 

Figure A.1.1. Wall Construction: a) Partial Walls; b) Horizontal Reinforcement Placement


a)


b)

Figure A.1.2. Wall Construction: a) Half Wall; b) Full Wall

a)

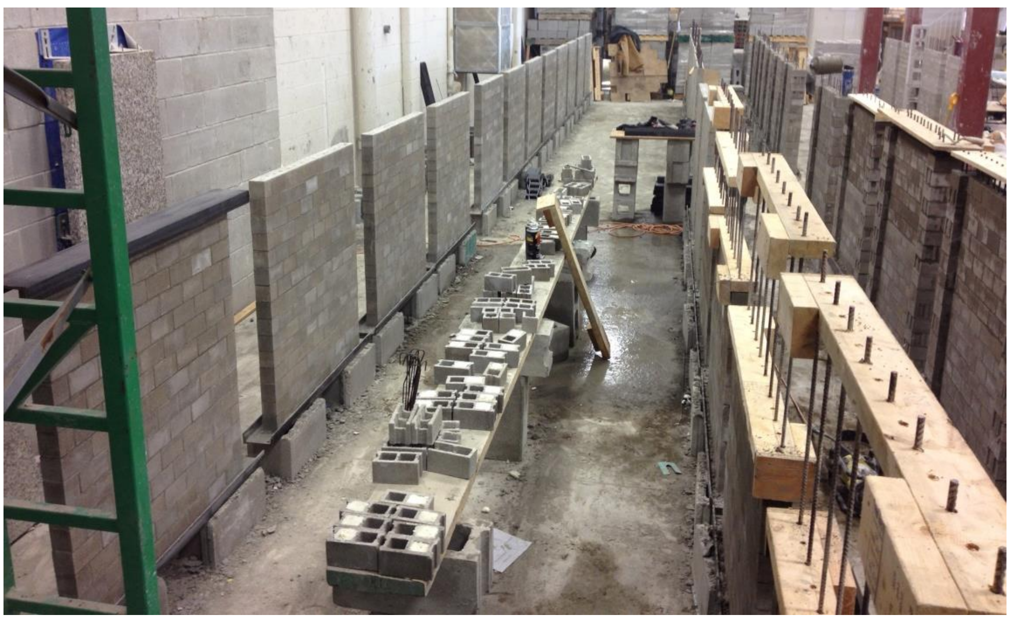

b)

Figure A.1.3. Wall Construction Overview: a) Half Walls; b) Full Walls

A.2 Blast Test Setup

Figure A.2.1. Loaded Supplies at Blast Test Site

Figure A.2.2. Test Site before Placement of Bunkers

Figure A.2.3. Test Site after Bunker Placement

Figure A.2.4. Blast Test Bunkers Facing Charge

Figure A.2.5. Instrumentation Tent

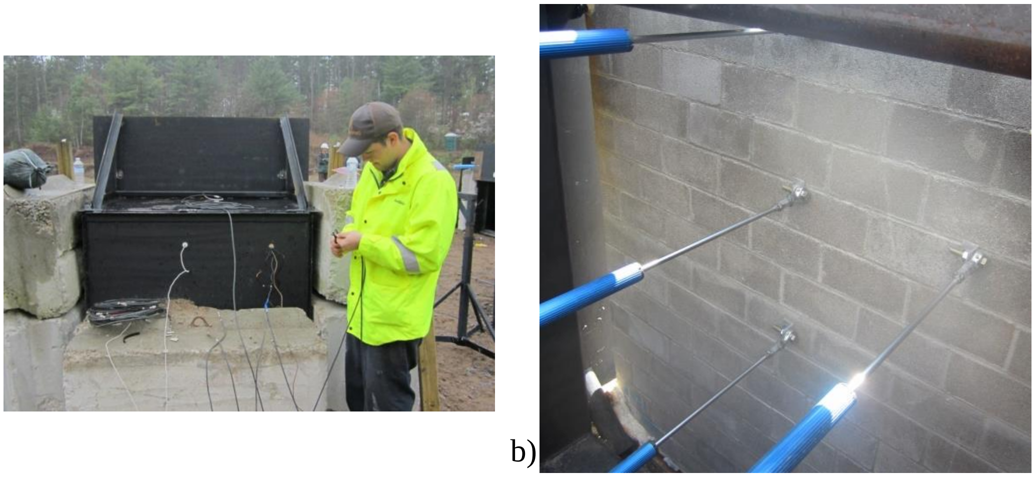

a) b)

Figure A.2.6. Blast Test Setup: a) Wiring Instrumentation; b) LVDTs on Wall

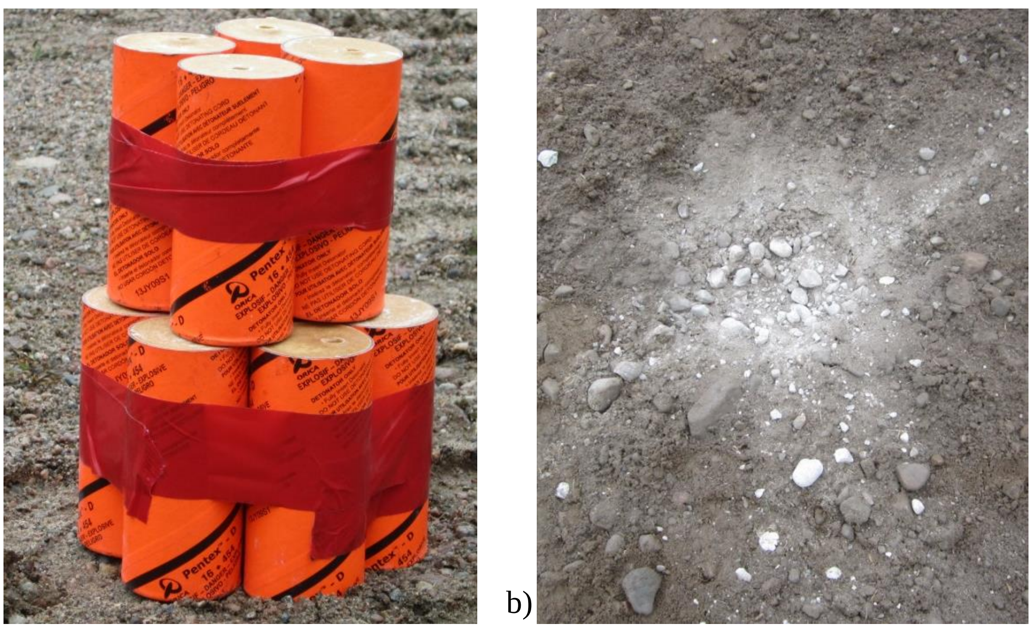

a) b)

Figure A.2.7. Blast Test Setup: a) Explosive Charge; b) Crater from Explosive

A.3 Static Test Setup


a)

b)

Figure A.3.1. Static Test Setup: a) Airbag;
b) Airbag between Wall and Reaction Frame


a)

b)

Figure A.3.2. Reaction Frame: a) Front View ; b) Rear View

APPENDIX B – THEORETICAL STATIC CAPACITIES

The following outlines the procedures used to calculate the flexural and shear capacities of the infill walls under static loading conditions.

B.1 Flexural Capacity

To calculate the flexural capacity, each specimen was treated in a similar manner to that of a reinforced concrete slab developing a two-way, out-of-plane flexural response. The yield line theory using the virtual work method (Park and Gamble 2000) was used by assuming the development of yield lines at the critical locations observed during the experimental testing as depicted in Fig. B.1.1-a. Due to symmetry of the specimens, the capacity formulation can be calculated by equating the internal and external work for a quarter of the specimen area. The relative peak displacement of the diagonal yield line can vary between values of one-half and the full displacement at the centre of the wall. For the purpose of simplification, this value was assumed to be one-half in this analysis although more refined values can be used.

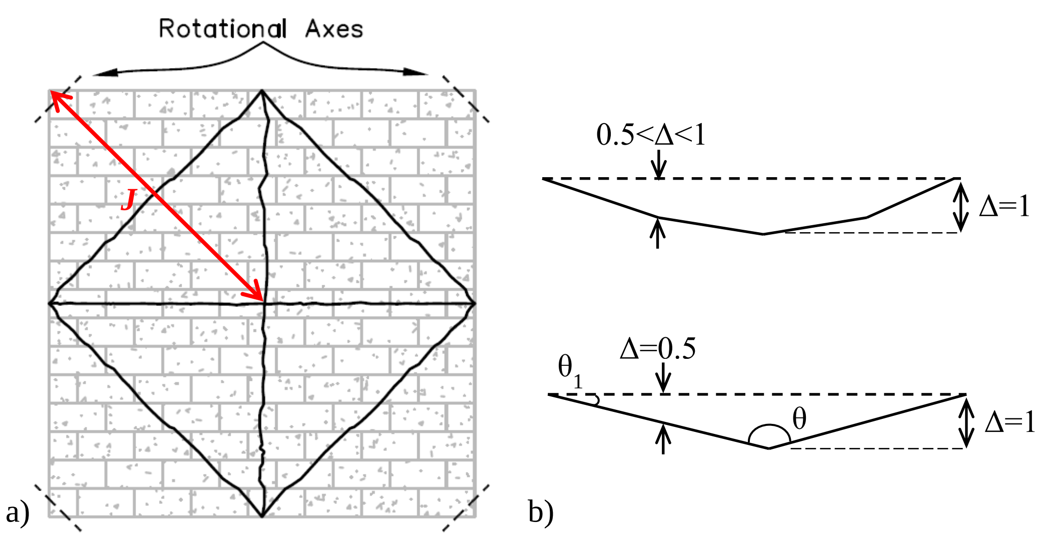

Figure B.1.1. Flexural Failure Pattern: a) Layout; b) Rotation Depiction

Determination of Capacity Equation:

Support rotation resulting from a unit displacement (Δ=1) at the centre point:

$$\theta_1 = {}^{\Delta}\!/_{J} = {}^{1}\!/_{\frac{L}{\sqrt{2}}} = \frac{\sqrt{2}}{L} \quad \text{(B.1.1)}$$

$$\theta = 2\theta_1 = \frac{2\sqrt{2}}{L} \quad \text{(B.1.2)}$$

Internal Work:

$$V = mJ\theta = m\frac{L}{\sqrt{2}}\frac{2\sqrt{2}}{L} = 2m \quad \text{(B.1.3)}$$

External Work:

$$U = qa\delta$$
$$= q\frac{1}{2}\left(\frac{L}{2}\right)^2\frac{2}{3}*\frac{1}{2} + q\frac{1}{2}\left(\frac{L}{2}\right)^2\frac{2}{3}*1$$
$$= \frac{1}{24}qL^2 + \frac{1}{12}qL^2$$
$$= \frac{1}{8}qL^2 \quad \text{(B.1.4)}$$

Equating Internal and External Work:

$$U = V$$
$$\frac{1}{8}qL^2 = 2m$$
$$\therefore q = 16m \quad \textit{or} \quad \mathbf{W_{fl}} = {}^{\mathbf{16M_u}}\!/_{\mathbf{L^2}} \quad \text{(B.1.5)}$$

Calculation of Section Ultimate Moment Resistance (M_u):

The out-of-plane ultimate moment resistance (M_u) is calculated by using the equivalent stress block procedure, outlined in CSA S304.1-04.

Section Compressive and Tensile Forces:

$$C = 0.85f'_m b\beta_1 c \quad \text{(B.1.6)}$$
$$T = A_s f_s \leq A_s f_y \quad \text{(B.1.7)}$$

Sample Calculation for WNL Wall Type:

A_s = 200 mm^2
b = 1000 mm
d = 31.67 mm
β_1 = 0.8
f'_m = 18.2 mPa
F_y = 478 mPa
ε_y = 0.00206 mm/mm

Assuming reinforcing steel yields;

$$C = T$$
$$A_s f_y = 0.85 f'_m b \beta_1 c$$
$$200 * 478 = 0.85 * 18.2 * 1000 * 0.8 * c$$
$$c = 7.72\ mm$$

ε_s = 0.00922 mm/mm > ε_y; yielding assumption correct

$$M_u = A_s f_y \left(d - \frac{\beta_1 c}{2}\right) \tag{B.1.8}$$
$$= 200 * 478 \left(31.67 - \frac{0.8 * 7.72}{2}\right)$$
$$= 2.73\ kN.m$$

Table B.1.1. Wall Flexural Capacities

Wall	***M_u* (kN.m)**	***W_{fl}* (kPa)**
WNL	2.73	43.68
WNM	4.64	74.24
WNH	6.18	98.88

B.2 Shear Capacity

At the critical shear locations, the shear forces are to be resisted through a combination of a bond and shear-friction mechanisms. These methods of shear resistance are used in both masonry (CSA S304.1-04) and reinforced concrete (CSA A23.3-04) design codes.

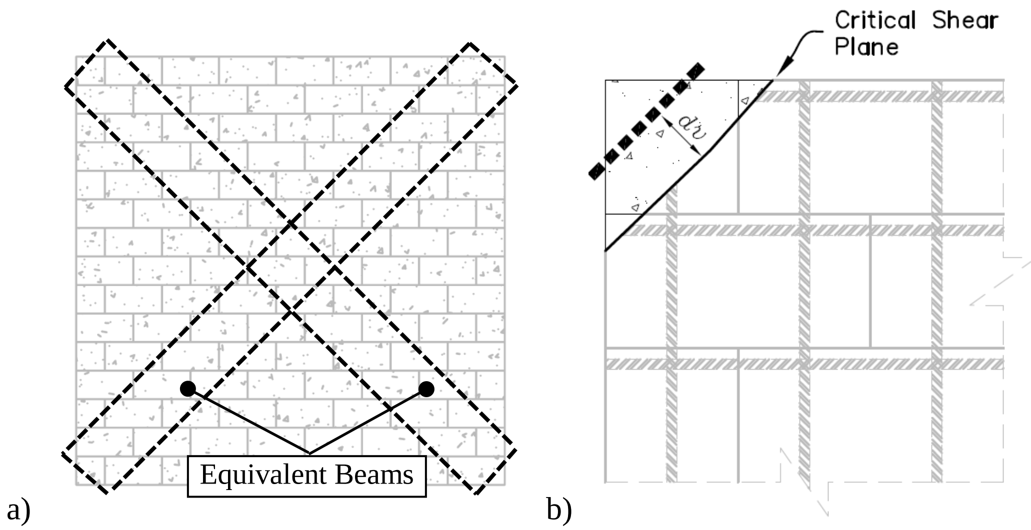

Figure B.2.1. Shear Failure Pattern: a) Equivalent Beams; b) Critical Section

Determination of Capacity Equation:

Simplifying the shear behaviour of the walls to act as beams spanning diagonally between the supports (Fig. B.2.1-a), it becomes apparent that the critical shear plane will be at a distance d_v from the support and parallel to the assumed axis of rotation as depicted in Fig. B.2.1-b. For the cross section of the walls, d_v is assumed to be half the wall thickness (31 mm), which represents the distance measured from the extreme compression fibre to the centroid of the steel reinforcement located at the middle of the wall.

The maximum shear resistance is calculated by:

$$V_r = C_o A_e + \mu A_{sv} f_{sc} \qquad \text{(B.2.1)}$$

where C_o is the masonry bond resistance, estimated as:

$$C_o = \frac{f'_m + f'_t}{f'_m * f'_t} \qquad \text{(B.2.2)}$$

Assuming the support reactions act as point loads at each corner (Fig. B.2.2), equilbirum of the forces is used to estimate the load capacity of the wall specimens that was result in a shear dominated failure mode.

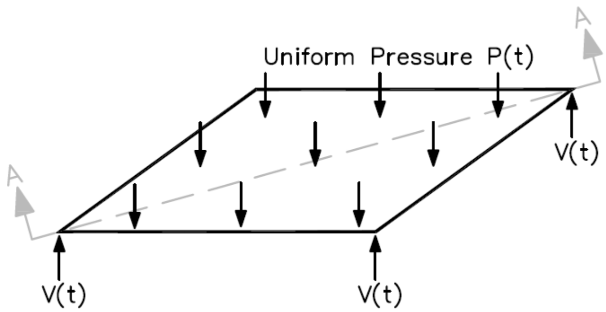

Figure B.2.2. Forces Acting on Walls

$$4V_r - W_{sh} * A = 0 \quad \text{(B.2.3)}$$

∴ The equivalent load capacity for a shear dominated failure in the wall specimens is estimated to be:

$$\boldsymbol{W_{sh}} = {}^{\boldsymbol{4V_r}}/_{\boldsymbol{A}} \quad \text{(B.2.4)}$$

<u>Sample Calculation for WNL Wall Type:</u>

A_e = 15207 mm^2
μ = 1.0
f'_m = 18.2 MPa
A_{sv} = 96 mm^2
f_{sc} = 60 MPa*
$f'_t \approx 0.6\sqrt{f'_m}$; as per CSA A23.3-04, assuming fully grouted wall acts similar to reinforced concrete

**Note:* f_{sc} determined to be maximum stress in reinforcement at the critical shear location coinciding with the initial yield at the centre of the wall.

$$C_o = \frac{f'_m + f'_t}{f'_m * f'_t} = \frac{f'_m + 0.6\sqrt{f'_m}}{f'_m * 0.6\sqrt{f'_m}} = 2.24\ MPa$$

$$V_r = C_o A_e + \mu A_{sv} f_{sc}$$
$$= 2.24 * 15207 + 1.0 * 96 * 60$$
$$= 39824\ N\ or\ 39.8\ kN$$

And the equivalent load capacity for a shear dominated failure is;

$$W_{sh} = {}^{4V_r}/_{A} = {}^{4 * 39.8\ kN}/_{1\ m^2} = 159.2\ kPa$$

Table B.2.1. Wall Shear Capacities

Wall	V_r **(kN)**	W_{sh} **(kPa)**
WNL	39.8	159.2
WNM	44.9	179.6
WNH	53.5	214.0

B.3 Notation:

The following symbols are used in this Appendix:

a = Loaded surface area;
A = Total surface area of wall;
A_e = Effective masonry area along critical shear plane, equal to length of shear crack multiplied by wall thickness;
A_s = Area of steel reinforcement;
A_{sv} = Area of longitudinal steel passing through critical shear plane;
b = Width of cross section;
c = Depth of neutral axis;
C = Compressive force;
C_o = Bond (cohesive) resistance provided by masonry;
d = Distance between reinforcement and extreme compression fibre;
f'_m = Masonry compressive strength;
f'_t = Masonry tensile strength;
f_s = Reinforcement stress;
f_{sc} = Clamping stress provided by longitudinal reinforcement;
f_y = Reinforcement yield strength;
J = Moment arm from support to centre of wall;
L = Length of square wall;

m	=	Yield line moment;
M_u	=	Ultimate out-of-plane moment capacity of the masonry wall;
q	=	Uniform surface pressure on loaded area;
T	=	Tensile force;
V_r	=	Shear resistance;
W_{fl}	=	Flexural capacity;
W_{sh}	=	Shear capacity;
β_1	=	Equivalent stress block constant;
δ	=	Centroid displacement of loaded area;
Δ	=	Unit displacement at centre of wall;
ε_s	=	Reinforcement strain;
ε_y	=	Reinforcement yield strain;
μ	=	Friction coefficient;
θ	=	Total rotation at centre of wall;
θ_1	=	Support Rotation